

Scattering of transient waves by an interface with time-modulated jump conditions

Michaël Darche^a, Raphael Assier^b, Sébastien Guenneau^{c,d}, Bruno Lombard^{a,*}, Marie Touboul^{e,c,f}

^a*Aix Marseille Université, CNRS, Centrale Marseille, LMA UMR 7031, Marseille, France*

^b*Department of Mathematics, University of Manchester, Oxford Road, Manchester M13 9PL, UK*

^c*UMI 2004 Abraham de Moivre-CNRS, Imperial College London, London SW7 2AZ, UK*

^d*Department of Physics, The Blackett Laboratory, Imperial College London, London SW7 2AZ, UK*

^e*Department of Mathematics, Imperial College London, Huxley Building, Queen's Gate, London SW7 2AZ, UK*

^f*POEMS, ENSTA Paris, CNRS, INRIA, Institut Polytechnique de Paris, 91120, Palaiseau, France*

Abstract

Time modulation of the physical parameters offers new possibilities for wave control. Examples include amplification of waves, harmonic generation and non-reciprocity, without resorting to non-linear mechanisms. Most of the recent studies on the matter focus on the time-modulation of the physical properties of a given media, that is, a time-modulation ‘in volume’. Here, we focus instead on time modulation at some lower-dimensional space by considering time-varying jump conditions across some interface. The latter offers simpler solutions for practical implementation. This work is focused on wave propagation in a 1D medium containing one modulated interface. Many properties of the scattered waves are investigated theoretically: energy balance, generation of harmonics, impedance matching and non-reciprocity. A fourth-order numerical method is also developed to simulate such transient scattering. Numerical experiments are conducted to validate both the theoretical findings and the numerical scheme.

Keywords: Elastic waves, Imperfect jump conditions, Time-varying media, Non-reciprocity, Numerical methods for hyperbolic PDE

1. Introduction

Since the early 2000s, periodic modulation of physical properties in space has led to significant developments in wave control. Based on homogenization theory and Floquet-Bloch analysis, these so-called *metamaterials* have made it possible to achieve cloaking, negative refraction or perfect lensing, to cite a few of the exotic effects. We refer the interested reader to [14] for an overview of this abundant subject in the case of acoustics.

In recent years, the technical possibility of modulating physical properties in time has opened new perspectives in the field of metamaterials [8, 9, 22]. Time-varying metamaterials exhibit unusual phenomena such as time reflection and time refraction, nontrivial topology [52, 37],

*Corresponding author. Tel.: +33 491 84 52 42 53.

Email addresses: `darche@lma.cnrs-mrs.fr` (Michaël Darche), `raphael.assier@manchester.ac.uk` (Raphael Assier), `s.guenneau@imperial.ac.uk` (Sébastien Guenneau), `lombard@lma.cnrs-mrs.fr` (Bruno Lombard), `marie.touboul@ensta.fr` (Marie Touboul)

frequency conversion [50] unidirectional and parametric amplification [58, 29, 28]. Numerous works have emerged since the late fifties, investigating this physics both theoretically [16, 43, 55, 11, 10, 18, 12, 61, 38, 35, 39, 26, 57, 27, 51, 17, 63, 42, 45, 2, 1, 46, 25, 19, 24, 48, 30, 59] and experimentally [3, 13, 31, 53, 20, 40, 54, 56, 44, 36, 23]. In particular, systems that are periodically modulated in both space and time, have the ability to alleviate some of the constraints of static media, such as the breaking of reciprocity. As a result, exciting wave control possibilities have been identified, such as unidirectional amplification [62], coherent perfect absorption [21] and non-reciprocity [15, 47, 54].

Nevertheless, a current limitation relies on the difficulty to achieve time modulation of bulk parameters experimentally (e.g. density or Young's modulus of elasticity). It is easier to modify properties at discrete points, for example, by modifying the stiffness of a membrane or a surface impedance [65, 64]. Recent work has focused on the experimental realization of these devices, and on the theoretical analysis of wave propagation using multiple scattering [49] or transmission-line theory [41].

The aim of this paper is then to study theoretically and numerically the propagation of waves across a time-modulated interface. For this purpose, the article is structured as follows. Section 2 describes the model at hand: time-dependent jump conditions, which generalize the jump conditions widely used to describe imperfect contacts [4]. Interface dissipation is also incorporated to be closer to experimental devices. An energy balance is conducted. The generation of harmonics is studied through a harmonic balance analysis. The particular case of reflectionless modulated interface is discussed. Section 3 describes the time-domain numerical methods for first-order systems. A fourth-order finite-difference ADER scheme is used. The main novelty concerns the discretization of time-varying jump conditions, which involves a modification of the Explicit Simplified Interface Method (ESIM) [32, 33]. Validation of the numerical results is done by comparisons with a semi-analytical solution. Section 4 presents different numerical experiments, illustrating the theoretical findings: amplification of waves, generation of harmonics, impedance matching, and non-reciprocity. Lastly, Section 5 draws future lines of research such as homogenization of a network of such modulated interfaces.

2. Physical modeling

2.1. Problem statement

Let us consider a one-dimensional linear elastic medium with density $\rho(x)$ and Young's modulus $E(x) = \rho(x) c^2(x)$, where c is the sound speed (the analysis is however relevant to other wave physics problems such as acoustics or s-polarization and p-polarization in electromagnetism, see Remark 1). These parameters may be discontinuous at $x = x_0$. The conservation of momentum and the Hooke's law are formulated as follows:

$$\begin{cases} \partial_t(\rho(x) \partial_t u(x, t)) = \partial_x \sigma(x, t) + F(x, t), & (1a) \\ \sigma(x, t) = E(x) \partial_x u(x, t), & (1b) \end{cases}$$

with u being the displacement field, σ the stress field, and F a body force with compact support that does not contain x_0 . The velocity field is denoted by $v = \partial_t u$. For any function $g(x)$, we define the jump and mean operators $[[\cdot]]_{x_0}$ and $\langle\langle \cdot \rangle\rangle_{x_0}$ as

$$[[g]]_{x_0} = g^+(x_0) - g^-(x_0), \quad \langle\langle g \rangle\rangle_{x_0} = \frac{1}{2} (g^+(x_0) + g^-(x_0)), \quad (2)$$

where

$$g^\pm(x_0) = \lim_{\eta \rightarrow 0^+} g(x_0 \pm \eta). \quad (3)$$

To simplify the notations, the indices and arguments denoting space and time will be omitted when no risk of ambiguity occurs; in particular, x_0 is omitted in the jump and mean operators from now on. As can be seen from direct computations, for any two functions f and g , these operators satisfy the property

$$\llbracket gh \rrbracket = \llbracket g \rrbracket \langle\langle h \rangle\rangle + \langle\langle g \rangle\rangle \llbracket h \rrbracket. \quad (4)$$

Introducing interface parameters of stiffness $\mathcal{K}(t) > 0$, compliance $\mathcal{C}(t) = 1/\mathcal{K}(t)$, inertia $\mathcal{M}(t) \geq 0$ and dissipation $\mathcal{Q}_{C,M} \geq 0$, the imperfect interface is modelled by the time-dependent jump conditions:

$$\begin{cases} \llbracket v(\cdot, t) \rrbracket = \partial_t (\mathcal{C}(t) \langle\langle \sigma(\cdot, t) \rangle\rangle) + \mathcal{Q}_C \langle\langle \sigma(\cdot, t) \rangle\rangle, \\ \llbracket \sigma(\cdot, t) \rrbracket = \partial_t (\mathcal{M}(t) \langle\langle v(\cdot, t) \rangle\rangle) + \mathcal{Q}_M \langle\langle v(\cdot, t) \rangle\rangle. \end{cases} \quad (5a)$$

$$(5b)$$

Five remarks arise from (5):

- The modulated jump conditions are assumed to result from an external stimulus (photoelastic effect, piezoelectric components, etc.);
- As seen further in Section 2.2, the compliance $\mathcal{C}(t)$ and the inertia $\mathcal{M}(t)$ must be *inside* the time derivative to ensure a sound energy balance;
- For the sake of simplicity and realism, the dissipation parameters \mathcal{Q}_C and \mathcal{Q}_M are assumed to be static. The terms in (5a) are reminiscent of the Maxwell model of viscoelasticity;
- When $\mathcal{C} \rightarrow 0$, $\mathcal{Q}_C = 0$, $\mathcal{M} = 0$ and $\mathcal{Q}_M = 0$, one recovers the conditions of perfect bonding.
- If $\mathcal{Q}_C = 0$, then (5a) can be recast in the more usual form with displacement:

$$\llbracket u(\cdot, t) \rrbracket = \mathcal{C}(t) \langle\langle \sigma(\cdot, t) \rangle\rangle;$$

Remark 1. *The problem studied in this article is generic to various wave physics problems. For instance, the case of acoustics is obtained by changing u into the acoustic pressure, E into the inverse of mass density and ρ into the compressibility. Similarly, the case of s -polarization (resp. p -polarization) in electromagnetism can be obtained by changing u into the transverse electric (resp. magnetic) field, ρ into the permittivity (resp. permeability) and E into the inverse of the permeability (resp. inverse of the permittivity).*

2.2. Energy balance

We take the product of the momentum equation (1a) by $v = \partial_t u$ and integrate over $(-\infty, x_0)$. Integrating by parts and using (1b) give

$$\begin{aligned} \int_{-\infty}^{x_0} \rho v \partial_t v dx &= \int_{-\infty}^{x_0} v \partial_x \sigma dx + \int_{-\infty}^{x_0} F v dx, \\ &= - \int_{-\infty}^{x_0} \sigma \partial_x v dx + [v \sigma]_{-\infty}^{x_0} + \int_{-\infty}^{x_0} F v dx, \\ &= - \int_{-\infty}^{x_0} \frac{1}{E} \sigma \partial_t \sigma dx + v^-(x_0, t) \sigma^-(x_0, t) + \int_{-\infty}^{x_0} F v dx. \end{aligned} \quad (6)$$

Similarly, integrating over $(x_0, +\infty)$ yields

$$\int_{x_0}^{+\infty} \rho v \partial_t v dx = - \int_{x_0}^{+\infty} \frac{1}{E} \sigma \partial_t \sigma dx - v^+(x_0, t) \sigma^+(x_0, t) + \int_{x_0}^{+\infty} F v dx, \quad (7)$$

where we have used the fact that F is compactly supported and that the fields vanish at infinity. Summing (6) and (7) leads to

$$\frac{d}{dt} \left(\frac{1}{2} \int_{\mathbb{R}} \left(\rho v^2 + \frac{1}{E} \sigma^2 \right) dx \right) = - \llbracket v \sigma \rrbracket + \int_{\mathbb{R}} F v dx. \quad (8)$$

The property (4) and the jump conditions (5) lead to

$$\begin{aligned} \llbracket v \sigma \rrbracket &= \llbracket v \rrbracket \langle\langle \sigma \rangle\rangle + \langle\langle v \rangle\rangle \llbracket \sigma \rrbracket, \\ &= (\mathcal{C}'(t) \langle\langle \sigma \rangle\rangle + \mathcal{C}(t) \langle\langle \partial_t \sigma \rangle\rangle + \mathcal{Q}_C \langle\langle \sigma \rangle\rangle) \langle\langle \sigma \rangle\rangle + (\mathcal{M}'(t) \langle\langle v \rangle\rangle + \mathcal{M}(t) \langle\langle \partial_t v \rangle\rangle + \mathcal{Q}_M \langle\langle v \rangle\rangle) \langle\langle v \rangle\rangle, \\ &= \frac{d}{dt} \left(\frac{1}{2} (\mathcal{C}(t) \langle\langle \sigma \rangle\rangle^2 + \mathcal{M}(t) \langle\langle v \rangle\rangle^2) \right) + \frac{1}{2} (\mathcal{C}'(t) \langle\langle \sigma \rangle\rangle^2 + \mathcal{M}'(t) \langle\langle v \rangle\rangle^2) + \mathcal{Q}_C \langle\langle \sigma \rangle\rangle^2 + \mathcal{Q}_M \langle\langle v \rangle\rangle^2. \end{aligned} \quad (9)$$

It leads to the following energy balance.

Proposition 1. *Let $\mathcal{E}_m = \mathcal{E}_b + \mathcal{E}_i$ be the total energy, with the bulk energy*

$$\mathcal{E}_b(t) = \frac{1}{2} \int_{\mathbb{R}} \left(\rho v^2 + \frac{1}{E} \sigma^2 \right) dx \quad (10)$$

and the interface energy

$$\mathcal{E}_i(t) = \frac{1}{2} \mathcal{M} \langle\langle v \rangle\rangle^2 + \frac{1}{2} \mathcal{C} \langle\langle \sigma \rangle\rangle^2. \quad (11)$$

Introducing the power of external forces due to body forcing

$$\mathcal{P}(t) = \int_{\mathbb{R}} F v dx, \quad (12)$$

one has

$$\frac{d}{dt} \mathcal{E}_m(t) = \mathcal{P}(t) - \frac{1}{2} (\mathcal{M}'(t) \langle\langle v \rangle\rangle^2 + \mathcal{C}'(t) \langle\langle \sigma \rangle\rangle^2) - (\mathcal{Q}_C \langle\langle \sigma \rangle\rangle^2 + \mathcal{Q}_M \langle\langle v \rangle\rangle^2). \quad (13)$$

Five remarks arise from Proposition 1 and positivity of \mathcal{M} , \mathcal{C} , \mathcal{Q}_C and \mathcal{Q}_M :

- both \mathcal{E}_b and \mathcal{E}_i are positive, hence $\mathcal{E}_m \geq 0$;
- in \mathcal{E}_i one recognizes the kinetic energy and the potential energy of a spring-mass system when static parameters are considered;
- if there are no body force ($F = 0$), no time-modulation (both \mathcal{M} and \mathcal{C} are constant in time) and no dissipation term in the jump conditions ($\mathcal{Q}_C=0$ and $\mathcal{Q}_M=0$), then the total mechanical energy is conserved;

- if no body force is applied ($F = 0$) and both \mathcal{M} and \mathcal{C} are constant in time, but \mathcal{Q}_C or \mathcal{Q}_M is non-zero, then the total mechanical energy is dissipated;
- if $F = 0$ but either \mathcal{M} or \mathcal{C} vary with time, then the total mechanical energy may vary, due to the power of external forces required to modify \mathcal{M} and \mathcal{C} . The sign of the right-hand-side in (13) is arbitrary, so that \mathcal{E}_m may increase or decrease.

The latter remark about the amplification of energy raises the question of possible parametric amplification. Under suitable assumptions, the next Proposition states that such an amplification is not possible, and that the solution remains bounded. The proof is given in Appendix Appendix C.

Proposition 2. *Let us assume:*

- (i) *a sinusoidal modulation of the interface compliance $\mathcal{C}(t)$;*
- (ii) *no jump of stress (ie $\mathcal{M}(t) = 0$ and $\mathcal{Q}_M = 0$);*
- (iii) *a body force in (1a) in the form $F(x, t) = \delta(x - x_s) S(t)$, where S is bounded.*

Then the scattered fields v and σ remain bounded for all t .

This result is counter-intuitive, since modulated systems often exhibit resonance (e.g. a modulated spring-mass system). An interpretation is that the energy may be evacuated on both sides of the domain, preventing from an unbounded increase. A similar conclusion holds by interchanging the roles of \mathcal{C} and \mathcal{M} . The case where both interface compliance and interface inertia are modulated remains open, though our numerical experiments suggest that the same result will hold in this case.

2.3. Generation of harmonics

The interaction of a single-frequency wave with a modulated interface generates an infinite number of harmonics. Here we shortly describe how to compute them. For simplicity, constant physical parameters are considered around the interface at $x_0 = 0$. In this part, a sinusoidal modulation for \mathcal{C} and \mathcal{M} is chosen:

$$\begin{aligned}\mathcal{C}(t) &= \mathcal{C}_0 (1 + \varepsilon_C \sin(\Omega t)), \\ \mathcal{M}(t) &= \mathcal{M}_0 (1 + \varepsilon_M \sin(\Omega t)),\end{aligned}\tag{14}$$

with $\Omega = 2\pi f_m$, where f_m is the modulation frequency, and $\mathcal{C}_0 \geq 0$, $\mathcal{M}_0 \geq 0$ and $-1 < \varepsilon_{C,M} < 1$. A harmonic incident wave v^{in} and σ^{in} of the form

$$v^{\text{in}}(x, t) = e^{i\omega(t-x/c)}; \quad \sigma^{\text{in}}(x, t) = -\rho c e^{i\omega(t-x/c)}$$

impacts the interface from the left. Thus, we can write

$$v^{\text{tot}}(x, t) = \begin{cases} v^{\text{in}}(x, t) + v^{\text{ref}}(x, t) & \text{for } x < 0 \\ v^{\text{trans}}(x, t) & \text{for } x > 0, \end{cases}$$

and

$$\sigma^{\text{tot}}(x, t) = \begin{cases} \sigma^{\text{in}}(x, t) + \sigma^{\text{ref}}(x, t) & \text{for } x < 0 \\ \sigma^{\text{trans}}(x, t) & \text{for } x > 0, \end{cases}$$

for some reflected and transmitted wave fields v^{ref} , σ^{ref} , v^{trans} and σ^{trans} that also satisfy the governing wave equation. These fields should look like

$$v^{\text{ref}}(x, t) = \sum_{k \in \mathbb{Z}} R_k e^{i\omega_k(t+x/c)}, \quad \sigma^{\text{ref}}(x, t) = \rho c \sum_{k \in \mathbb{Z}} R_k e^{i\omega_k(t+x/c)}, \quad (15)$$

$$v^{\text{trans}}(x, t) = \sum_{k \in \mathbb{Z}} T_k e^{i\omega_k(t-x/c)}, \quad \sigma^{\text{trans}}(x, t) = -\rho c \sum_{k \in \mathbb{Z}} T_k e^{i\omega_k(t-x/c)}, \quad (16)$$

for some reflection and transmission coefficients R_k and T_k to be determined, and where we denote $\omega_k \equiv \omega + k\Omega$. One introduces the auxiliary quantities $\Psi_k = T_k - R_k$ and $\Phi_k = T_k + R_k$.

2.3.1. Dealing with the first jump equation

Using (15) and (16), together with the definition of the jump operator, we find that

$$\llbracket v^{\text{tot}} \rrbracket = e^{i\omega t} \left(-1 + \sum_{k \in \mathbb{Z}} \Psi_k e^{ik\Omega t} \right) \quad \text{and} \quad \langle\langle \sigma^{\text{tot}} \rangle\rangle = -\frac{\rho c}{2} e^{i\omega t} \left(1 + \sum_{k \in \mathbb{Z}} \Psi_k e^{ik\Omega t} \right).$$

Similarly, though it is slightly longer, we find that

$$\begin{aligned} \partial_t \langle\langle \mathcal{E}(t) \sigma^{\text{tot}} \rangle\rangle &= e^{i\omega t} \left(\frac{\mathcal{C}\varepsilon_C}{4} \omega_{-1} e^{-i\Omega t} - \frac{i\mathcal{C}}{2} \omega - \frac{\mathcal{C}\varepsilon_C}{4} \omega_1 e^{+i\Omega t} \right) \\ &+ e^{i\omega t} \sum_{k \in \mathbb{Z}} \left(-\frac{\mathcal{C}\varepsilon_C}{4} \omega_k \Psi_{k-1} - \frac{i\mathcal{C}}{2} \omega_k \Psi_k + \frac{\mathcal{C}\varepsilon_C}{4} \omega_k \Psi_{k+1} \right) e^{ik\Omega t}, \end{aligned}$$

where we have introduced the reduced quantity $\mathcal{C} = \rho c \mathcal{C}_0$. Therefore the first jump condition (5a), after dividing through by $e^{i\omega t}$ and rearranging slightly becomes

$$\begin{aligned} \sum_{k \in \mathbb{Z}} \left(\frac{\mathcal{C}\varepsilon_C}{4} \omega_k \Psi_{k-1} + \left(1 + \frac{\mathcal{Q}_C}{2} + i\frac{\mathcal{C}}{2} \omega_k \right) \Psi_k - \frac{\mathcal{C}\varepsilon_C}{4} \omega_k \Psi_{k+1} \right) e^{ik\Omega t} \\ = \frac{\mathcal{C}\varepsilon_C}{4} \omega_{-1} e^{-i\Omega t} + \left(1 - \frac{\mathcal{Q}_C}{2} - i\frac{\mathcal{C}\omega}{2} \right) - \frac{\mathcal{C}\varepsilon_C}{4} \omega_1 e^{+i\Omega t}, \end{aligned} \quad (17)$$

where $\mathcal{Q}_C = \rho c \mathcal{Q}_C$. Since the $e^{ik\Omega t}$ functions are linearly independent, we obtain this system in matrix form:

$$\mathbb{A}(\mathcal{C}, \varepsilon_C, \mathcal{Q}_C, \omega, \Omega) \mathbf{\Psi} = \mathbf{V}(\mathcal{C}, \varepsilon_C, \mathcal{Q}_C, \omega, \Omega), \quad (18)$$

where

$$\begin{aligned} \mathbf{\Psi} &\equiv (\dots \Psi_{-N}, \dots \Psi_{-1}, \Psi_0, \Psi_1, \dots \Psi_N, \dots)^\top, \\ \mathbf{V}(\mathcal{C}, \varepsilon_C, \mathcal{Q}_C, \omega, \Omega) &= \left(\dots 0 \dots \frac{\mathcal{C}\varepsilon_C}{4} \omega_{-1}, 1 - \frac{\mathcal{Q}_C}{2} - i\frac{\mathcal{C}}{2} \omega, -\frac{\mathcal{C}\varepsilon_C}{4} \omega_1, \dots 0 \dots \right)^\top, \end{aligned} \quad (19)$$

and \mathbb{A} is a tri-banded antidiagonal matrix. Now we can truncate this system so that \mathbb{A} becomes a $(2N+1) \times (2N+1)$ matrix, and the truncated vector $\mathbf{\Psi}$ can be recovered by simple inversion.

2.3.2. Dealing with the second jump equation

One obtains directly

$$\llbracket \sigma^{\text{tot}} \rrbracket = \rho c e^{i\omega t} \left(1 - \sum_{k \in \mathbb{Z}} \Phi_k e^{ik\Omega t} \right) \quad \text{and} \quad \langle\langle v^{\text{tot}} \rangle\rangle = \frac{1}{2} e^{i\omega t} \left(1 + \sum_{k \in \mathbb{Z}} \Phi_k e^{ik\Omega t} \right).$$

Similarly, we find that

$$\begin{aligned} \partial_t \langle\langle \mathcal{M}(t) v^{\text{tot}} \rangle\rangle &= e^{i\omega t} \left(-\frac{\mathcal{M}_0 \varepsilon_M}{4} \omega_{-1} e^{-i\Omega t} + \frac{i\mathcal{M}_0}{2} \omega + \frac{\mathcal{M}_0 \varepsilon_M}{4} \omega_1 e^{+i\Omega t} \right) \\ &+ e^{i\omega t} \sum_{k \in \mathbb{Z}} \left(\frac{\mathcal{M}_0 \varepsilon_M}{4} \omega_k \Phi_{k-1} + \frac{i\mathcal{M}_0}{2} \omega_k \Phi_k - \frac{\mathcal{M}_0 \varepsilon_M}{4} \omega_k \Phi_{k+1} \right) e^{ik\Omega t}. \end{aligned}$$

Upon introducing $\mathcal{M} = \mathcal{M}_0 / (\rho c)$ and $\mathcal{Q}_M = \mathcal{Q}_M / (\rho c)$, the second jump condition (5b) leads to

$$\begin{aligned} \sum_{k \in \mathbb{Z}} \left(\frac{\mathcal{M} \varepsilon_M}{4} \omega_k \Phi_{k-1} + \left(1 + \frac{\mathcal{Q}_M}{2} + i \frac{\mathcal{M}}{2} \omega_k \right) \Phi_k - \frac{\mathcal{M} \varepsilon_M}{4} \omega_k \Phi_{k+1} \right) e^{ik\Omega t} \\ = \frac{\mathcal{M} \varepsilon_M}{4} \omega_{-1} e^{-i\Omega t} + \left(1 - \frac{\mathcal{Q}_M}{2} - i \frac{\mathcal{M} \omega}{2} \right) \Phi_0 - \frac{\mathcal{M} \varepsilon_M}{4} \omega_1 e^{+i\Omega t}. \end{aligned} \quad (20)$$

We end up with a system of the form

$$\mathbb{B}(\mathcal{M}, \varepsilon_M, \mathcal{Q}_M, \omega, \Omega) \boldsymbol{\Phi} = \mathbf{W}(\mathcal{M}, \varepsilon_M, \mathcal{Q}_M, \omega, \Omega). \quad (21)$$

The matrix \mathbb{B} and the vector \mathbf{W} are obtained by replacing $(\mathcal{C}, \varepsilon_C, \mathcal{Q}_C, \omega, \Omega)$ by $(\mathcal{M}, \varepsilon_M, \mathcal{Q}_M, \omega, \Omega)$ in \mathbb{A} and \mathbf{V} . The vector $\boldsymbol{\Phi}$ is

$$(\dots, \Phi_{-N}, \dots, \Phi_{-1}, \Phi_0, \Phi_1, \dots, \Phi_N, \dots)^\top.$$

As before, this system can be solved for any truncation by simple inversion.

2.3.3. Final reflection and transmission coefficients

Once Ψ_k and Φ_k are computed, the reflection and transmission coefficients are given by:

$$R_k = \frac{1}{2} (\Phi_k - \Psi_k), \quad T_k = \frac{1}{2} (\Psi_k + \Phi_k). \quad (22)$$

Two limit-cases are highlighted:

- Without modulation, the only non-zero coefficients are R_0 and T_0 . These coefficients are given in Appendix Appendix A;
- If $\mathcal{M} = \mathcal{C}$, $\varepsilon_M = \varepsilon_C$ and $\mathcal{Q}_C = \mathcal{Q}_M$, then the two matrix systems (18) and (21) are exactly the same, and so $\boldsymbol{\Phi} = \boldsymbol{\Psi}$, which leads to $R_k = 0$ for all k . This property of *impedance matching* is summarized in the following proposition.

Proposition 3. *Let us consider a homogeneous medium of impedance Z . If the three equalities*

$$\mathcal{M}_0 = Z^2 \mathcal{C}_0, \quad \mathcal{Q}_M = Z^2 \mathcal{Q}_C, \quad \varepsilon_C = \varepsilon_M, \quad (23)$$

hold, then no reflected wave is generated at the modulated interface.

Proposition 3 generalizes the impedance matching condition already obtained with static jump conditions and no dissipation in [4].

Remark 2. *Proposition 3 can be extended to any periodic modulation, while respecting $\mathcal{M}(t) = Z^2 \mathcal{C}(t)$, using the linearity of the equations and the fact that periodic functions can be decomposed into Fourier series.*

3. Numerical modeling

3.1. Numerical scheme

First-order formulation. A velocity-stress formulation of the evolution equations is used. We introduce the compact notations

$$\begin{aligned} \mathbf{U}(x, t) &= \begin{pmatrix} v(x, t) \\ \sigma(x, t) \end{pmatrix}, & \mathbf{F}(x, t) &= \begin{pmatrix} F(x, t) \\ \frac{F(x, t)}{\rho(x)} \\ 0 \end{pmatrix}, \\ \mathbf{A}(x) &= \begin{pmatrix} 0 & -\frac{1}{\rho(x)} \\ -E(x) & 0 \end{pmatrix}, & \mathbf{B}(t) &= \begin{pmatrix} 0 & \mathcal{C}(t) \\ \mathcal{M}(t) & 0 \end{pmatrix}, & \mathbf{E} &= \begin{pmatrix} 0 & \mathcal{Q}_C \\ \mathcal{Q}_M & 0 \end{pmatrix}, \end{aligned} \quad (24)$$

where \mathbf{A} and \mathbf{E} can be discontinuous at the interface. From (1) and from (5), one obtains the boundary-value problem

$$\begin{cases} \partial_t \mathbf{U} + \mathbf{A} \partial_x \mathbf{U} = \mathbf{F}, & x \neq x_0, \end{cases} \quad (25a)$$

$$\begin{cases} \llbracket \mathbf{U}(\cdot, t) \rrbracket = \partial_t (\mathbf{B}(t) \langle\langle \mathbf{U}(\cdot, t) \rangle\rangle) + \mathbf{E} \langle\langle \mathbf{U}(\cdot, t) \rangle\rangle. \end{cases} \quad (25b)$$

It is assumed that the body force is zero at the interface: $\mathbf{F}(x_0, t) = \mathbf{0}$, which is not restrictive.

ADER-4 scheme. A uniform grid with space step Δx and time step Δt is introduced, to determine an approximation \mathbf{U}_j^n of $\mathbf{U}(x_j = j \Delta x, t_n = n \Delta t)$. Integration of (25a) is done by a fourth-order ADER scheme. This explicit two-step finite-difference scheme is fourth-order accurate in space and time, using a stencil of 2 neighboring points on the right and on the left. It is stable under the usual CFL condition

$$\zeta = \max(c(x)) \frac{\Delta t}{\Delta x} \leq 1, \quad (26)$$

where $c(x) = \sqrt{\frac{E(x)}{\rho(x)}}$ is the sound speed. The reader is referred to [7] for implementation details.

3.2. Immersed interface method for time-modulated jump conditions

Discretization of the modulated jump conditions (25b) is done by implementing the Explicit Simplified Interface Method (ESIM). The philosophy of this numerical method is as follows: based on the jump conditions and the interface geometry, smooth extensions of the solution \mathbf{U} on either side of the interface are constructed at each time step (Figure 1). Evaluation of these extensions leads to modified values \mathbf{U}_j^* of the solution. At a point x_j on one side of the interface, the integration scheme (ADER 4 here) then uses the usual values \mathbf{U}_j^n if x_j is on the same side, and \mathbf{U}_j^* if x_j is on the other side of the interface. This method has been applied to various interface problems, notably to constant imperfect interfaces in 1D [32] and 2D [33].

An important ingredient of ESIM is to determine the jump conditions satisfied by the solution and its successive spatial derivatives. As the jump conditions here vary as a function of time, an important modification has to be made to the method, as detailed now. From (2) and (25b), we obtain

$$\mathbf{U}^+ - \frac{1}{2} \partial_t (\mathbf{B} \mathbf{U}^+) - \frac{1}{2} \mathbf{E}^+ \mathbf{U}^+ = \mathbf{U}^- + \frac{1}{2} \partial_t (\mathbf{B} \mathbf{U}^-) + \frac{1}{2} \mathbf{E}^- \mathbf{U}^-, \quad (27)$$

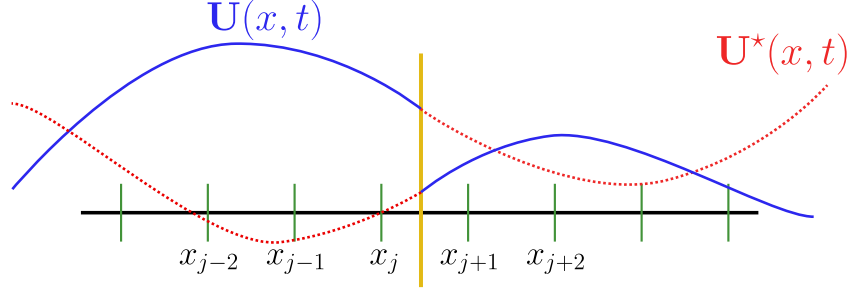


Figure 1: Scheme of the principle of ESIM at an interface with a discontinuous solution $\mathbf{U}(x, t)$ (blue line) and its smooth extensions $\mathbf{U}^*(x, t)$ (red dotted lines).

where the superscripts \pm refer to the limit values, as in (3). Using (25a), we then have

$$\left(\mathbf{I} - \frac{1}{2} (\partial_t \mathbf{B} + \mathbf{E}^+) \right) \mathbf{U}^+ + \frac{1}{2} \mathbf{B} \mathbf{A}^+ \partial_x \mathbf{U}^+ = \left(\mathbf{I} + \frac{1}{2} (\partial_t \mathbf{B} + \mathbf{E}^-) \right) \mathbf{U}^- - \frac{1}{2} \mathbf{B} \mathbf{A}^- \partial_x \mathbf{U}^-, \quad (28)$$

where \mathbf{I} is the 2×2 identity matrix. Successive time-differentiations of (28) up to an order k yields the matrix relation

$$\mathbf{C}_k^+(t) \mathbf{U}_k^+ + \mathbf{\Gamma}_{k+1}^+ = \mathbf{C}_k^-(t) \mathbf{U}_k^- + \mathbf{\Gamma}_{k+1}^-, \quad (29)$$

with the $2(k+1)$ vectors of limit values

$$\begin{aligned} \mathbf{U}_k^\pm &= (\mathbf{U}^\pm, \partial_x \mathbf{U}^\pm, \dots, \partial_x^k \mathbf{U}^\pm)^\top, \\ \mathbf{\Gamma}_{k+1}^\pm &= \left(\mathbf{0}, \mathbf{0}, \dots, \mathbf{0}, \mp \frac{(-1)^{k+1}}{2} \mathbf{B} (\mathbf{A}^\pm)^{k+1} \partial_x^{k+1} \mathbf{U}^\pm \right)^\top, \end{aligned} \quad (30)$$

where \mathbf{C}_k^\pm are $(2(k+1)) \times (2(k+1))$ time-dependent matrices, $\mathbf{0}$ is the 2×2 zero matrix, and $\mathbf{\Gamma}_{k+1}^\pm$ are $2(k+1)$ vectors. The matrices \mathbf{C}_k^\pm depend on the bulk parameters (through the matrices \mathbf{A}^\pm and \mathbf{E}^\pm) and the successive time derivatives of the jump conditions (through the matrix $\mathbf{B}(t)$ in (24)). Moreover, the matrices \mathbf{C}^\pm have a structure of block lower diagonal matrix; the 2×2 blocks below the diagonal depend on the successive time derivatives of $\mathcal{C}(t)$ and $\mathcal{M}(t)$.

Neglecting the $(k+1)$ -th spatial derivatives ($\mathbf{\Gamma}_{k+1}^\pm = \mathbf{0}_{2(k+1)}$) and inverting (29) yields

$$\begin{aligned} \mathbf{U}_k^+ &= (\mathbf{C}_k^+(t))^{-1} \mathbf{C}_k^-(t) \mathbf{U}_k^-, \\ &:= \mathbf{D}_k(t) \mathbf{U}_k^-. \end{aligned} \quad (31)$$

The transfer matrices $\mathbf{D}_k(t)$ of order k (31) are the building-block of the ESIM. These are used to calculate extrapolation matrices, which are used to determine the modified values \mathbf{U}_i^* at each time step. Once computed, the rest of the method follows the usual lines. The reader is referred e.g. to [60] for practical details. Four remarks can be made concerning the implementation and the properties of the ESIM:

- The transfer matrices \mathbf{D}_k in (31) depend on time. Consequently, the extrapolation matrices must be recalculated at each time step. This is an important difference with the cases previously dealt with by ESIM, where the extrapolation matrices were calculated once during a preprocessing step;

- The calculation of \mathbf{D}_k is tedious, especially for large values of k . A naive idea to simplify this calculation is to *freeze* the jump conditions at the instant under consideration, so that $\partial_t \mathbf{B} = \mathbf{0}$ in (28), and $\mathbf{D}_k(t)$ depends only on \mathbf{B} and not on its successive derivatives. This is a bad idea: the time evolution of the modulated interface conditions is then poorly described, leading to inaccurate numerical results;
- The problem under study has similarities with other time-varying interface problems. But here we are in a *kinematic* case, where the jump conditions are known and imposed, unlike *dynamic* cases such as [5], where the jump conditions are unknown and depend on the solution in a non-trivial way;
- The optimal choice of the derivation order k is important. In the case of static jump conditions (see e.g. [32]), a numerical analysis of the ESIM has been carried out, and we will reuse these results here. In the limit case where the interface disappears ($\mathcal{C}_0 \rightarrow 0$ and $\mathcal{M}_0 = 0$), $\mathbf{U}_j^* = \mathbf{U}_j^n$ is needed to recover the scheme in homogeneous medium. This consistency property is obtained if $k \geq s$, where s is the width of the stencil. Additionally, the local truncation error of a r -th order accurate scheme is maintained at the interface if $2k - 1 \geq r$. Putting together these two conditions yields

$$k = \max \left(s, r + 1 - \left\lfloor \frac{r + 1}{2} \right\rfloor \right), \quad (32)$$

where $\lfloor g \rfloor$ denotes the floor function of g . Here $s = 2$ and $r = 4$, so that $k = 3$ is the optimal value, which will be used in the numerical experiments. We will examine numerically the convergence properties using this value in Section 3.4 since we have no proof that it still holds in the current modulated case.

3.3. Numerical set-up

We consider a medium of length $L = 400$ m, with a modulated interface at $x_0 = 200$ m. The bulk parameters are constant: $\rho = 1200$ kg/m³ and $c = 2800$ m/s. The domain is discretized on $N_x = 400$ grid nodes. The CFL number in (26) is $\zeta = 0.95$.

Two types of forcing are considered: i) a Cauchy problem with an initial data associated with a right-going wave

$$\mathbf{U}(x, 0) = \begin{pmatrix} \rho \\ -1/c \end{pmatrix} S \left(t_0 - \frac{x}{c} \right), \quad (33)$$

where t_0 allows localizing the initial wave on the left of the interface, or ii) zero initial conditions with a time-dependent forcing at a Dirac source point

$$F(x, t) = S(t) \delta(x - x_s). \quad (34)$$

Both forcings involve the source function S , chosen as a combination of truncated sinusoids:

$$S(\xi) = \begin{cases} \sum_{m=1}^4 a_m \sin(b_m \omega_c \xi) & \text{if } -0 < \xi < 1/f_c \\ 0 & \text{otherwise,} \end{cases} \quad (35)$$

where $f_c = \omega_c/(2\pi)$ is the central frequency, $b_m = 2^{m-1}$, the coefficients a_m are $a_1 = 1$, $a_2 = -21/32$, $a_3 = 63/768$, and $a_4 = -1/512$. This source entails $C^6([0, +\infty[)$ smoothness. Figure 2 illustrates a Cauchy problem (a) and the spectral content of S (b).

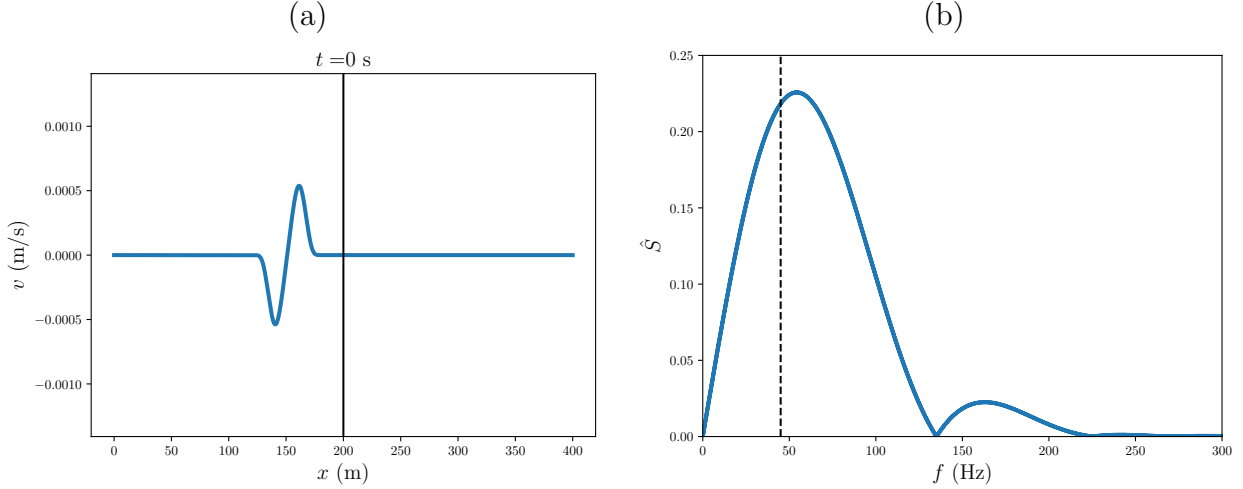


Figure 2: Forcing of simulations. (a) Cauchy problem (33) with $f_c = 45$ Hz. (b) Spectrum of the source (35); the vertical dotted line denotes the central frequency f_c .

The time dependence of \mathcal{C} and \mathcal{M} writes

$$\begin{aligned}\mathcal{C}(t) &= \mathcal{C}_0 (1 + \varepsilon_C \phi_C(t)), \\ \mathcal{M}(t) &= \mathcal{M}_0 (1 + \varepsilon_M \phi_M(t)),\end{aligned}\tag{36}$$

where $\mathcal{C}_0 \geq 0$, $\mathcal{M}_0 \geq 0$ and $\varepsilon_{C,M} \phi_{C,M} > -1$. The functions ϕ_C and ϕ_M may differ from each other. If $\phi_{C,M} = 0$ or $\varepsilon_{C,M} = 0$, then \mathcal{C} and \mathcal{M} do not depend on t , and one recovers the static conditions of imperfect contact investigated in [32]. In addition to the sinusoidal modulation (14), two modulation functions are introduced for the numerical simulations: a quasi-periodic modulation and a rectangular one. It follows

$$\phi_{C,M}(t) = \begin{cases} \sin(\Omega t), & \text{(sinusoidal),} \\ \sin(\Omega t) + \sin(\sqrt{2}\Omega t), & \text{(quasi-periodic),} \\ (-1)^n, \quad \text{with } n = \left\lfloor \left(\frac{\Omega t}{2\pi} \bmod 1 \right) - \nu \right\rfloor & \text{(rectangular),} \end{cases}\tag{37}$$

where $\lfloor g \rfloor$ denotes the floor function of g and $0 > \nu > 1$ and $\Omega = 2\pi f_m$, where f_m is the *modulation frequency*. In this work, we assume $\phi_C = \phi_M$ (which implies that the modulation frequencies are the same), but this is only for simplicity, and we could if we wanted to, without any modification of the code, use two completely different functions ϕ_C and ϕ_M .

3.4. Validation

In this part, a validation of the numerical scheme is proposed. A pulse is initially located on the left of the interface (33). The interface parameters are $\mathcal{K}_0 = 2.45$ GPa/m, $\mathcal{M}_0 = 0$, and the central frequency is $f_c = 30$ Hz. A semi-analytic solution of (25) can be obtained by the method of characteristics when $\mathcal{M}_0 = 0$ or $\mathcal{C}_0 = 0$. Technical details are given in Appendix Appendix B in the case where only the stiffness is modulated.

Figure 3-(a) and (b) illustrates the case without modulation: $\varepsilon_C = 0$. The other subfigures are computed using $\varepsilon_C = 0.9$ and various values of the modulation frequency $f_m = \frac{\Omega}{2\pi}$. Cases

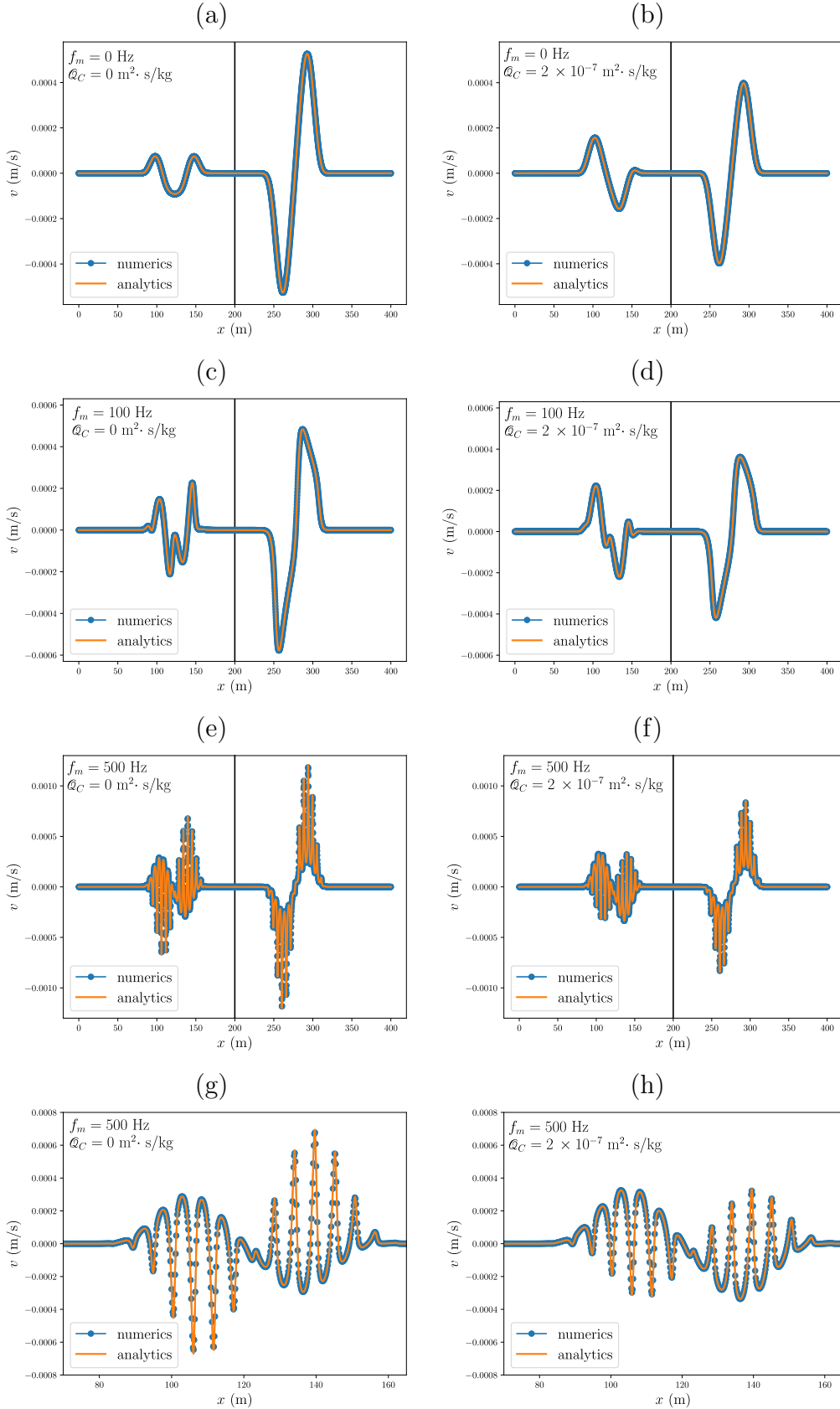


Figure 3: Scattering by an interface with modulated stiffness, for various frequencies of sinusoidal modulation f_m . Snapshot of the solution at $t = 0.045$ s with (a-b): no modulation, (c-d): $f_m = 100$ Hz, (e-f) $f_m = 500$ Hz, and (g-h) is a zoom on the reflected wave when $f_m = 500$ Hz. Left: cases without dissipation. Right: $Q_C = 2 \times 10^{-7} \text{ m}^2 \cdot \text{s}/\text{kg}$ and $Q_M = 0$.

without dissipation in the interface conditions ($\mathcal{Q}_C = 0$ and $\mathcal{Q}_M = 0$) are presented on the left column and cases with dissipation ($\mathcal{Q}_C = 2 \times 10^{-7} \text{ m}^2 \cdot \text{s} / \text{kg}$ and $\mathcal{Q}_M = 0$) are on the right side. The value of \mathcal{Q}_C have been chosen to have an effect of the same order as the compliance effect. One observes an excellent agreement between the exact and numerical values, which validates the numerical method detailed in Section 3. There is also an enrichment of peaks in the scattered waves when $|f_m - f_c|$ increases. In the rest of this work, we only consider cases with $\mathcal{Q}_C = 0$ and $\mathcal{Q}_M = 0$.

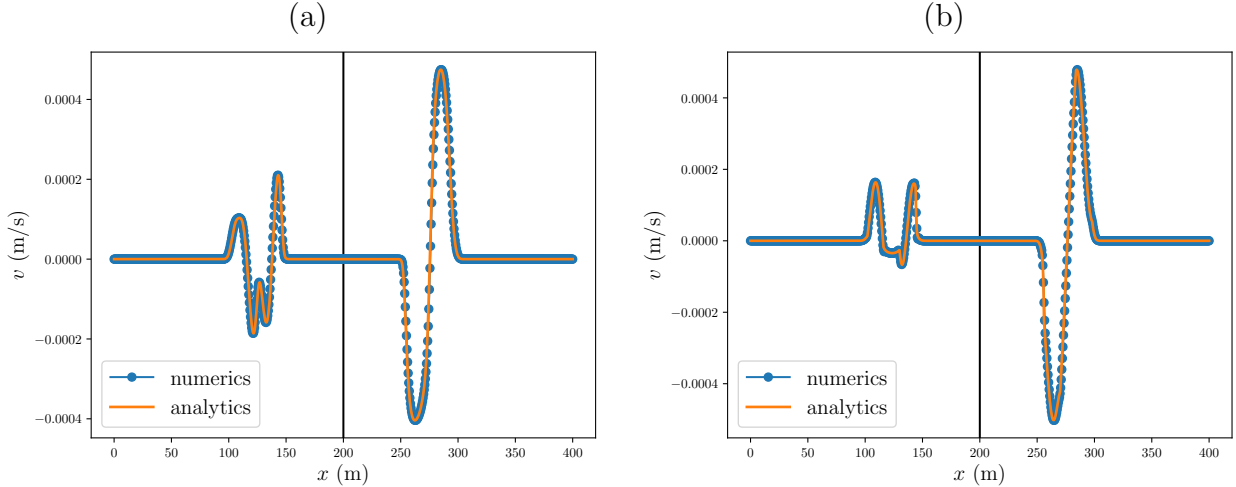


Figure 4: Scattering by an interface with modulated stiffness, for non-harmonic modulation at the frequency $f_m = 100$ Hz. (a): quasi-periodic modulation, (b): square modulation.

Figure 4 illustrates the two other modulation types given by (37) at the frequency $f_m = 100$ Hz. Figure 4-(a) displays the results obtained in the quasi-periodic modulation, while Figure 4-(b) investigates the rectangular modulation ($\nu = 0.65$ in (37)). Here again, there is an excellent agreement between the exact and numerical solution. It is important to notice that in the case of a square modulation, the terms corresponding to the derivatives of the modulation in (31) are set to zero.

Measures of convergence have been performed to verify the conclusions obtained in [32]. The Figure 5 presents the evolution of the error ε_v committed on the velocity field v at $t = 0.045$ s, and defined by:

$$\varepsilon_v = \sqrt{\Delta x \sum_{i=0}^{N_x} (v(x_i, t) - v_i^n)^2}. \quad (38)$$

On the left side, convergence measurement are shown for a sinusoidal modulation of the compliance \mathcal{C} using $\mathcal{K}_0 = 2.45 \text{ GPa} / \text{m}$ and $\mathcal{M} = 0$. On the right side, the analog case is presented (*i.e.* $\mathcal{M}_0 = 2 \times 10^4 \text{ kg} / \text{m}^2$ and $\mathcal{C} = 0$). The other numerical values of the parameters are $\varepsilon_{C,M} = 0.75$, $f_c = 45 \text{ Hz}$ and two different frequencies of a sine modulation are tested: $f_m = 100 \text{ Hz}$ (plain blue line) and $f_m = 10 \text{ Hz}$ (orange dashed line). These measurements show a convergence of order 4 for both modulations and both frequencies. The two curves corresponding to $f_m = 100 \text{ Hz}$ present a slope discontinuity for the higher value of Δx but we only consider the limit for small values of Δx . Moreover, due to the generation of harmonics with larger frequencies, the value of the error is more important for a modulation frequency at $f_m = 100 \text{ Hz}$ than at $f_m = 10 \text{ Hz}$.

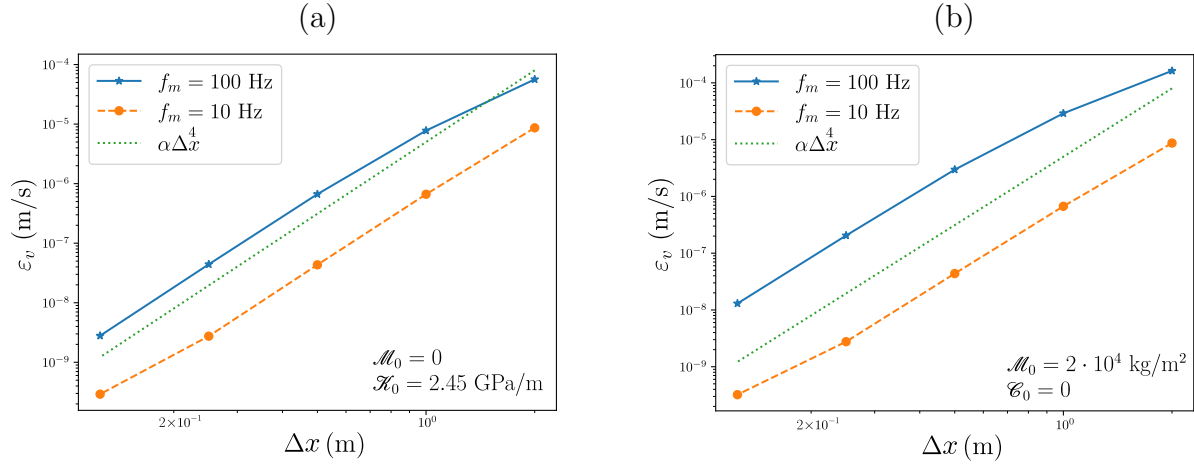


Figure 5: Convergence measurements for $f_m = 100$ Hz in blue line and $f_m = 10$ Hz in orange dashed line in the case where (a) $\mathcal{C}(t) \neq 0$ and $\mathcal{M}(t) = 0$, and (b) $\mathcal{C}(t) = 0$ and $\mathcal{M}(t) \neq 0$. The green dotted line shows a slope of order 4 (in log-log scale).

4. Numerical experiments

Here we illustrate the various properties analyzed in Section 2. We conclude with an illustration of non-reciprocity.

4.1. Modulation of energy

A pulse of the form (33) with central frequency $f_c = 45$ Hz is initially located on the left of the interface. The interface parameters are $\mathcal{K}_0 = 2.45$ GPa/m and $\mathcal{M}_0 = 2 \times 10^4$ kg/m² with a modulation frequency $f_m = 100$ Hz. Figure 6 investigates the scattered waves for different modulations. The left column shows a snapshot of the velocity v . The right column shows the temporal evolution of the energies (10)-(11) as a function of time. The background gray scale represents the time evolution of the interface parameters.

The total energy \mathcal{E}_m is constant until $t \approx 0.01$ s, when the incident wave impacts the interface. The initially zero interface energy \mathcal{E}_i then increases and remains non-zero as long as the wave/interface interaction lasts. As a consequence \mathcal{E}_m also varies. After the wave has passed through the interface, the interface energy is radiated and reconverted into bulk energy, which is then conserved. Depending on the sign of $\varepsilon_{C,M}$, different evolutions of energy are observed;

- In the first case $\varepsilon_{C,M} = 0.75$ (a-b), the final total energy value ($= 0.0013$) has almost doubled compared with the initial energy ($= 0.007$);
- In the second case, the modulation is inverted by choosing $\varepsilon_{C,M} = -0.75$ (c-d). The total amount of energy decreases from $= 0.007$ to $= 0.006$;
- In the third case, a rectangular modulation is applied with $\varepsilon_{C,M} = 0.75$ and $\nu = 0.65$ (e-f). The interface energy (and consequently the total energy) is then discontinuous.

In the first case, the interface is reached when the value of $\varepsilon_{C,M} \sin(\Omega t)$ is at its maximum value, whereas these values are negative in the second case. In conclusion, the work used to modulate the interface parameters can logically increase or decrease the total energy, as expected and predicted in our remarks to Proposition 1.

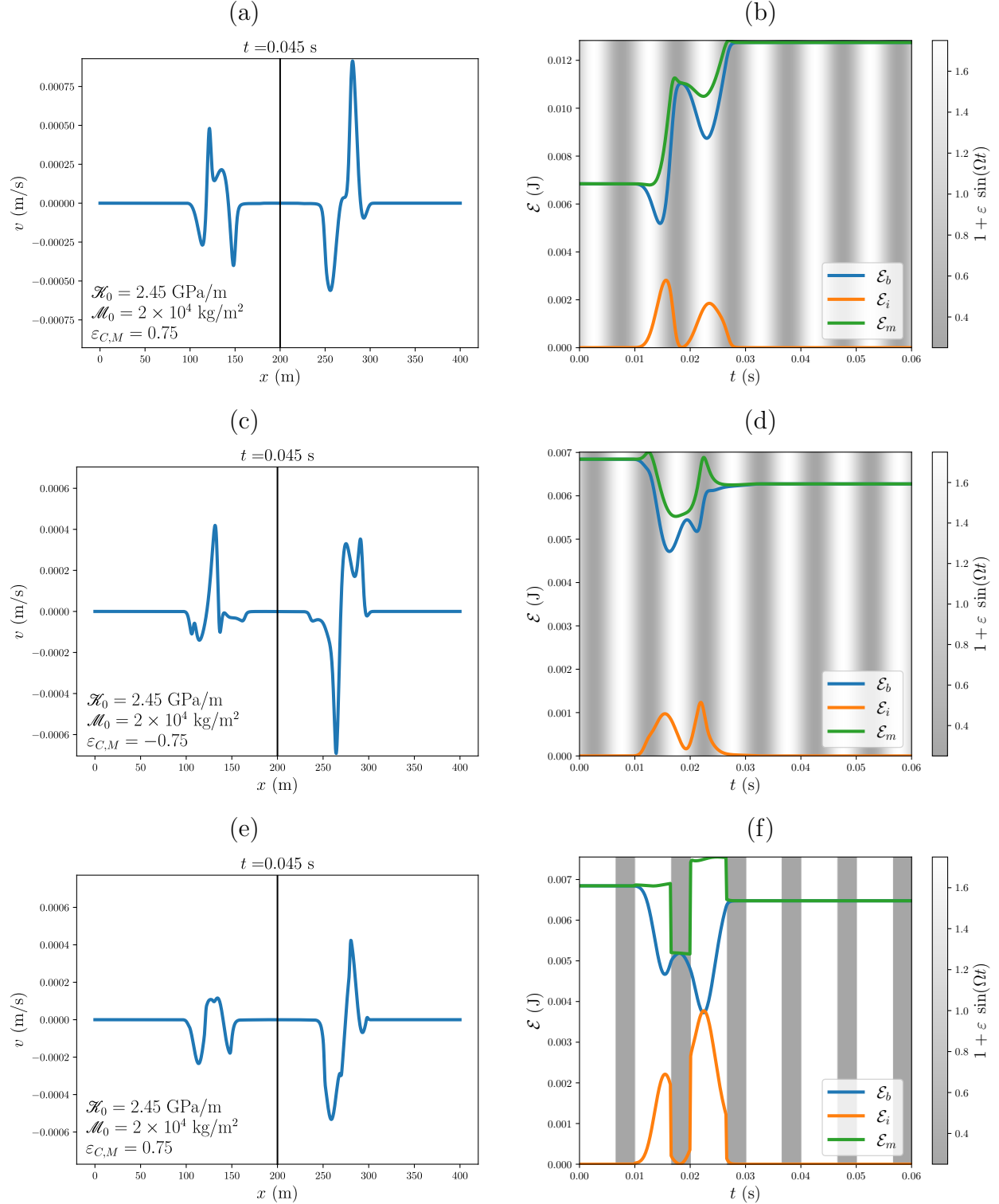


Figure 6: Interaction of a pulse centered on $f_c = 45$ Hz with a modulated interface. Left row: snapshot of the scattered velocity v at $t = 0.045$ s. Right row: time evolution of the energy, where the gray shaded areas denote the evolution of the interface parameters with modulation frequency $f_m = 100$ Hz. Sinusoidal modulation using (a-b): $\varepsilon_{C,M} = 0.75$; (c-d): $\varepsilon_{C,M} = -0.75$ and a rectangular modulation (e-f) with $\varepsilon_{C,M} = 0.75$ and $\nu = 0.65$.

4.2. Generation of harmonics

Here we illustrate the calculations carried out in Section 2.3. The reflection and transmission coefficients R_k and T_k in (15) are determined by solving (22) with $N = 12$ Fourier modes. This number has been chosen experimentally to ensure the convergence. The interface parameters are $\mathcal{K}_0 = 2.45$ GPa/m and $\mathcal{M}_0 = 2 \times 10^4$ kg/m², with modulation amplitudes $\varepsilon_C = \varepsilon_M = 0.75$.

The forcing is a Dirac source point (34) on the left of the interface ($x_s < x_0$). The velocity field is recorded at a receiver on the right of the interface ($x_r > x_0$), and then a FFT is performed. Three cases are studied considering different frequencies of the source ($f_c = \omega/(2\pi)$) and of the modulation ($f_m = \Omega/(2\pi)$). Their values are i) $f_c = 100$ Hz and $f_m = 30$ Hz in the first case, ii) $f_c = f_m = 30$ Hz in the second one, and iii) $f_c = 30$ Hz and $f_m = 100$ Hz in the third one.

Figure 7 compares the Fourier spectra of the reflected and transmitted signals obtained by FFT of direct simulations (blue lines) with the theoretical values obtained by harmonic balance (plain circles and stars). We represent here only the positive part of the frequencies as the spectrum is symmetric. The theoretical coefficient corresponding to negative (resp. positive) values of ω_k are then plotted in green circles (resp. purple stars). A vertical dotted line is set at the frequency f_c . In the three cases, the higher coefficient corresponds to the fundamental mode ($k = 0$) and the coefficient values decrease when $|k|$ increase. In each case, an excellent agreement is obtained between results of simulation and of harmonic balance, even for a small number of Fourier modes. The following observations are done:

- when $f_c > f_m$, the influence of negative frequencies is weak (almost zero) because it corresponds to higher modes. Moreover, the values of the coefficients decrease rapidly. The coefficients of the first harmonics are smaller than the half of the value at the frequency ω ;
- when $f_c = f_m$, then $\omega_{-1} = 0$ and the calculations show that $R_{-1} = T_{-1} = 0$. In this case, green circles and purple stars are located at the same frequency because $\omega_{-k} = \omega_{k-2}$ and in practice, the coefficients computed for $\omega_k < 0$ are strictly zero;
- when $f_c < f_m$, there is a stronger influence of the modes at negative frequencies. It can be explained by the fact that, as visible on the Figure 3, the signal is strongly modified with a high-frequency modulation. The first harmonic for the reflection coefficient is for example almost equal to the fundamental frequency (≈ 0.29), and there are twelve modes that can be noticed while only five or six were visible for a smaller modulation frequency.

4.3. Impedance matching

The interface is modulated sinusoidally at $f_m = 100$ Hz and its parameters are $\mathcal{M}_0 = 12 \times 10^3$ kg/m², $\mathcal{K}_0 = 941$ MPa/m, so that the properties (23) are verified. Both parameters are modulated at the same frequency and with the same amplitude $\varepsilon_{C,M} = 0.75$. Bulk parameters are given in Section 3.3.

Figure 8 illustrates the behavior of a wave at this modulated interface. On the left side, a snapshot of v is presented. At the left of the interface, no reflected wave propagates because of the impedance matching. The shape of the transmitted signal is similar to that obtained with the first configuration in Figure 6(a). As previously, the total amount of energy is modified when the pulse crosses the interface.

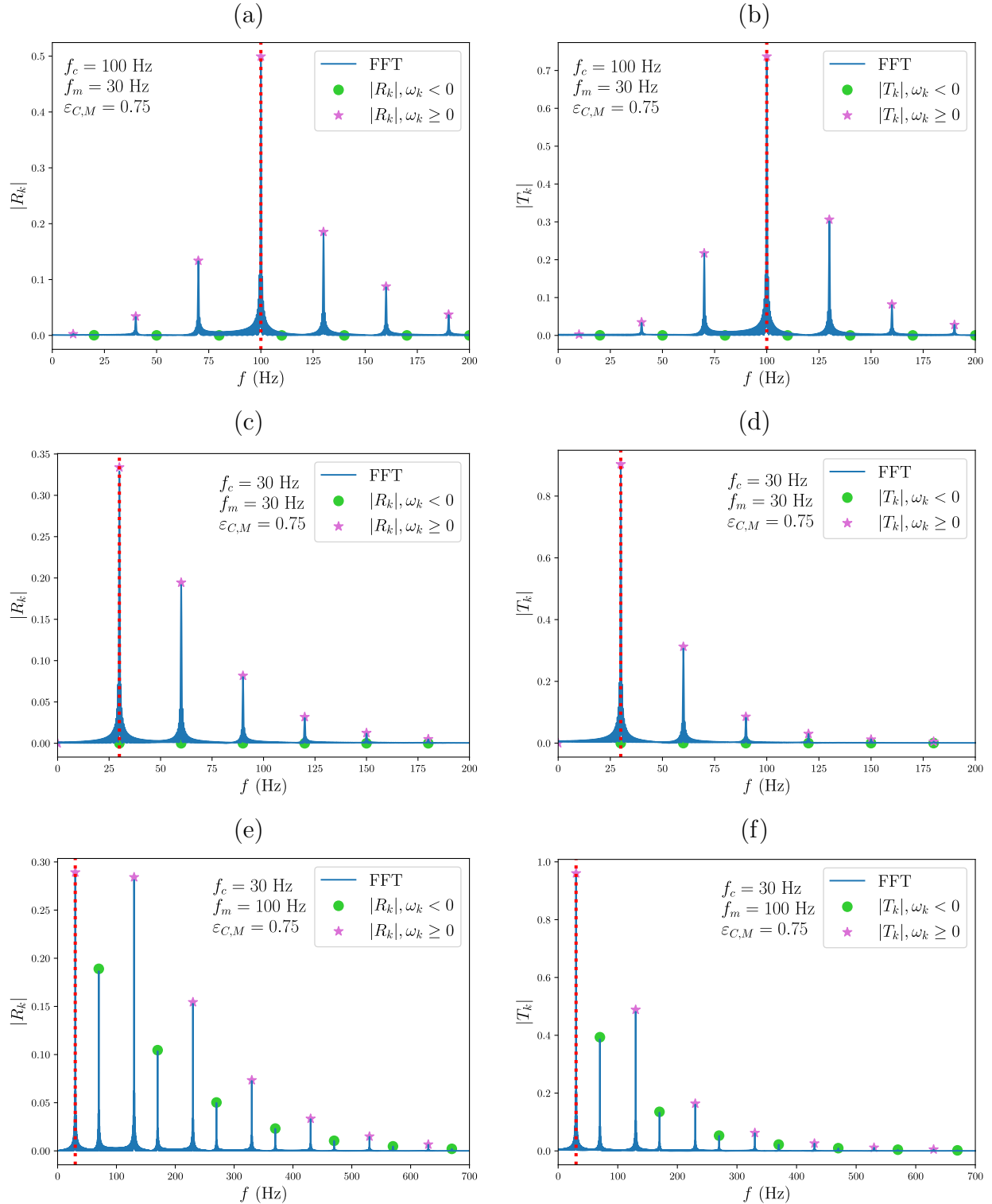


Figure 7: Generation of harmonics. Coefficients of reflection R_k (left row) and transmission T_k (right row) in (15). The vertical dotted line denotes the frequency f_c of the incident wave. (a-b): $f_c = 100$ and $f_m = 30$; (c-d): $f_c = f_m = 30$; (e-f): $f_c = 30$ and $f_m = 100$. Blue lines denote the FFT of direct simulations, whereas plain circles and plain stars denote the results of harmonic balance respectively for $\omega_k < 0$ and $\omega_k \geq 0$.

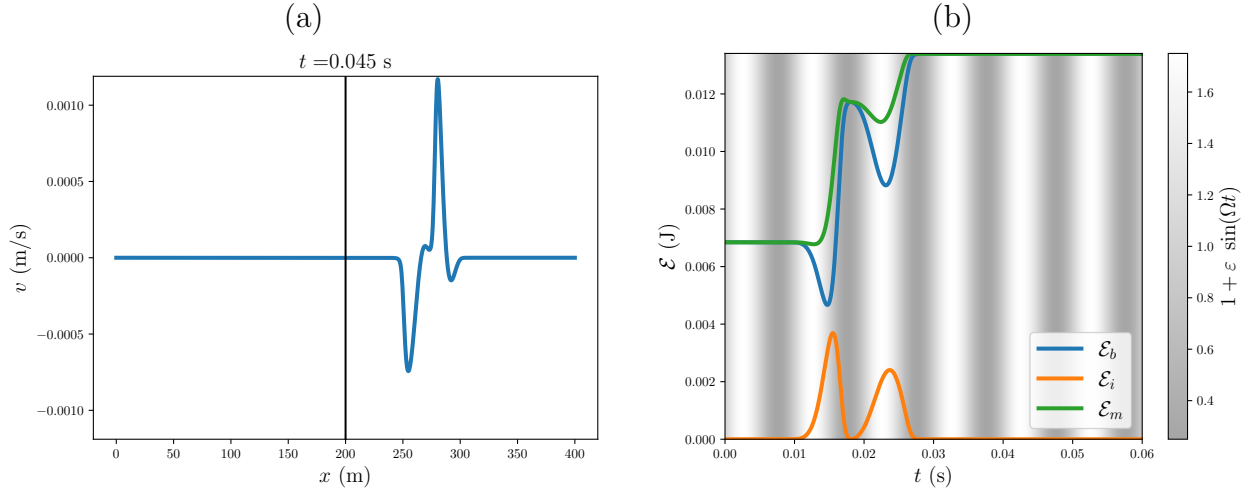


Figure 8: Reflectionless interaction of a pulse centered on $f_c = 45$ Hz with a modulated interface due to impedance adaptation. Left row: snapshot of the scattered velocity v at $t = 0.045$ s. Right row: time evolution of the energy, where the gray shaded areas denote the evolution of the interface parameters. The modulation function is sinusoidal.

Although the impedance matching (Proposition 3) has only been proven for the case of sinusoidal modulation, Figure 9 shows that the results can be extended to other functions defined by (37) if $\phi_C(t) = \phi_M(t)$. Two cases are tested: a quasi-periodic modulation with $f_m = 100$ Hz (a), and a rectangular modulation with $f_m = 100$ Hz and $\nu = 0.65$ (b). The latter case corresponds to the framework of Remark 2. In both cases, no reflection is observed.

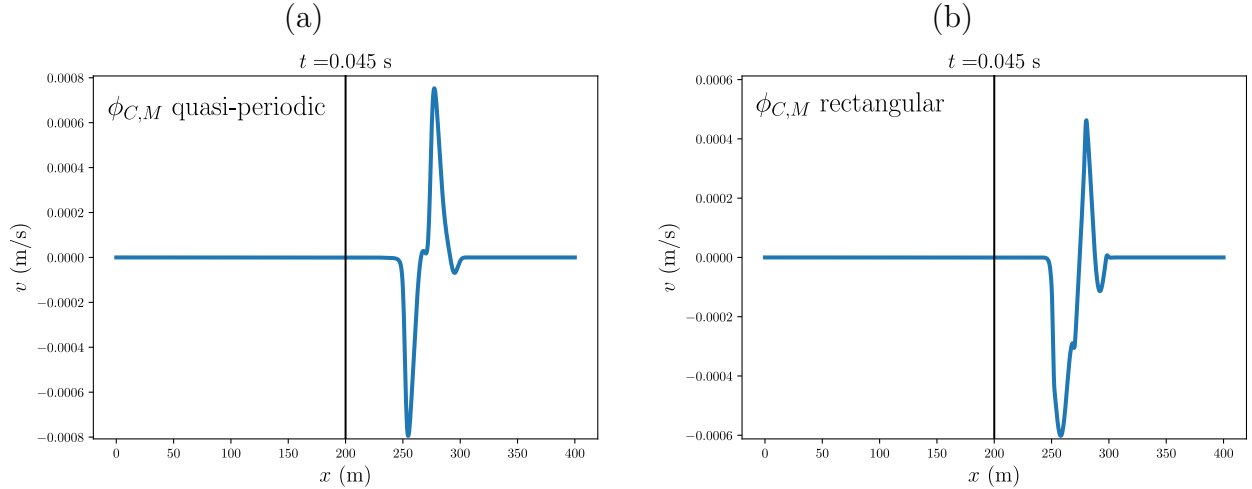


Figure 9: Snapshots of reflectionless interaction of a pulse centered on $f_c = 45$ Hz with a modulated interface at $t = 0.045$ s. Impedance adaptation (a) with a quasi-periodic modulation and (b) with a rectangular modulation.

4.4. Non-reciprocity

Lastly, we investigate numerically the non-reciprocity induced by time-modulating the parameters of the interface. The configuration is the same as in the previous Section. Figure 10 shows a comparison of temporal signals measured when we swap source and sensor (Figure

10(a)) for different values of f_c and f_m . The positions of the sources and sensors are $x_s = 150$ m and $x_r = 225$ m, respectively at a distance ℓ_s and ℓ_r to the interface.

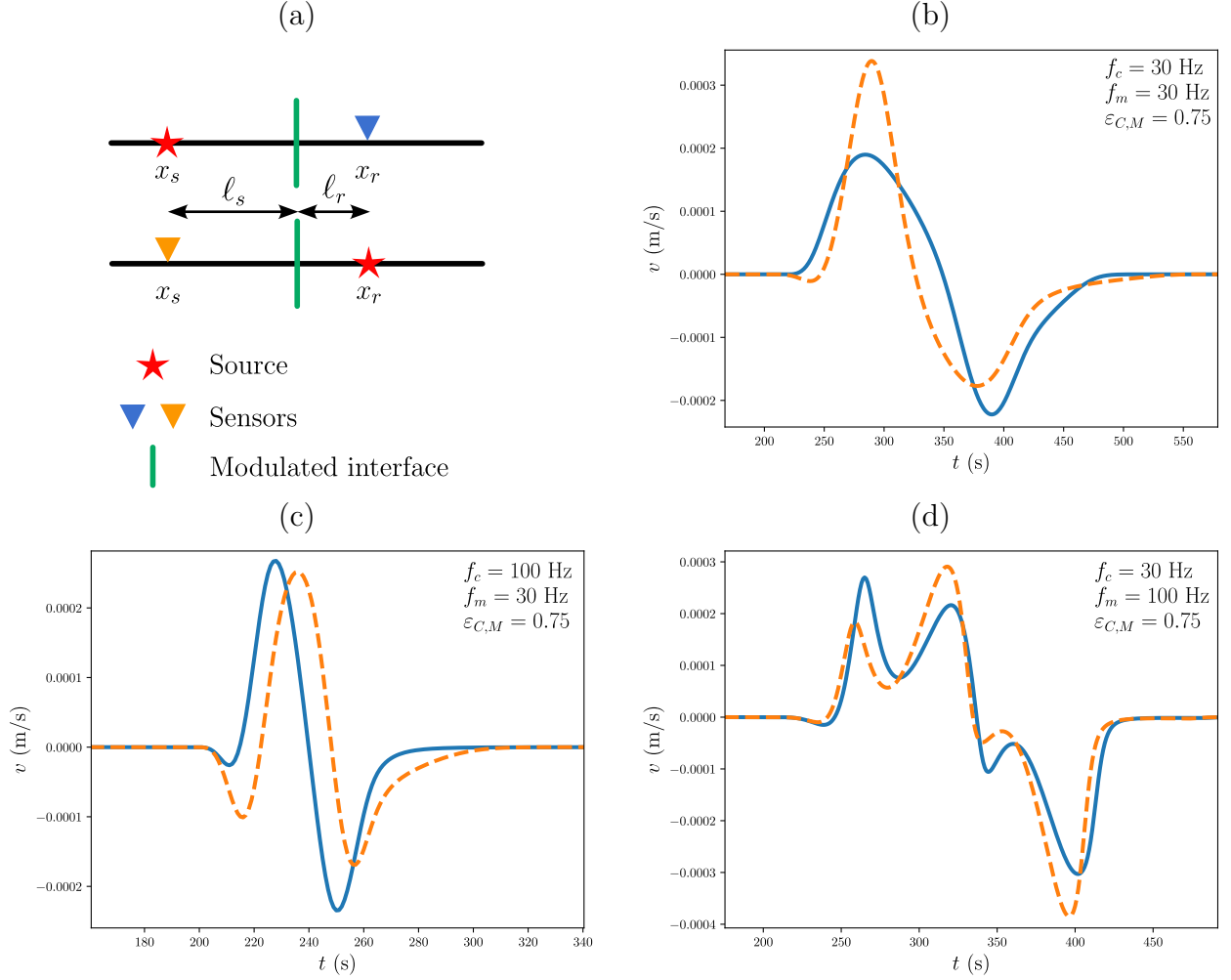


Figure 10: Illustration of non-reciprocity. (a) Scheme of the numerical experiment where the positions of the sensor and the source is inverted. The signals measured by the sensor are represented for (b) $f_m = f_c = 30$ Hz, (c) $f_c = 100$ Hz and $f_m = 30$ Hz and (d) $f_c = 30$ Hz and $f_m = 100$ Hz.

The transmission of waves through the interface is altered because of the change of state of the interface, when the wave reaches it. It is due to the difference in travel time from the source to the interface. In both cases, the measured signals are different, which illustrates the fact that the reciprocity theorem is no longer verified.

We propose in this Section to quantify the non-reciprocity by computing the difference between signals. Figure 11 presents a measure of the difference between the two signals v_s , measured by the sensor at $x = x_r$ due to the source in $x = x_s$, and v_r , measured by the sensor at $x = x_s$ due to the source in $x = x_r$ at $t = 0.07$ s. This quantity is defined by

$$\vartheta_v = f_c \sqrt{\sum_{i=0}^{N_x} (v_s - v_r)^2}. \quad (39)$$

Two types of modulation are studied, a sinusoidal one (14) and a quasi-periodic one (37) for 100 values of the modulation frequency f_m from 0 to 400 Hz. For the periodic modulation, two different frequencies of the pulse are tested: $f_c = 30$ Hz represented with the plain blue line and $f_c = 50$ Hz with orange dashed line. As the wavelength differs in the two cases, ϑ_v is normalized using the source frequency.

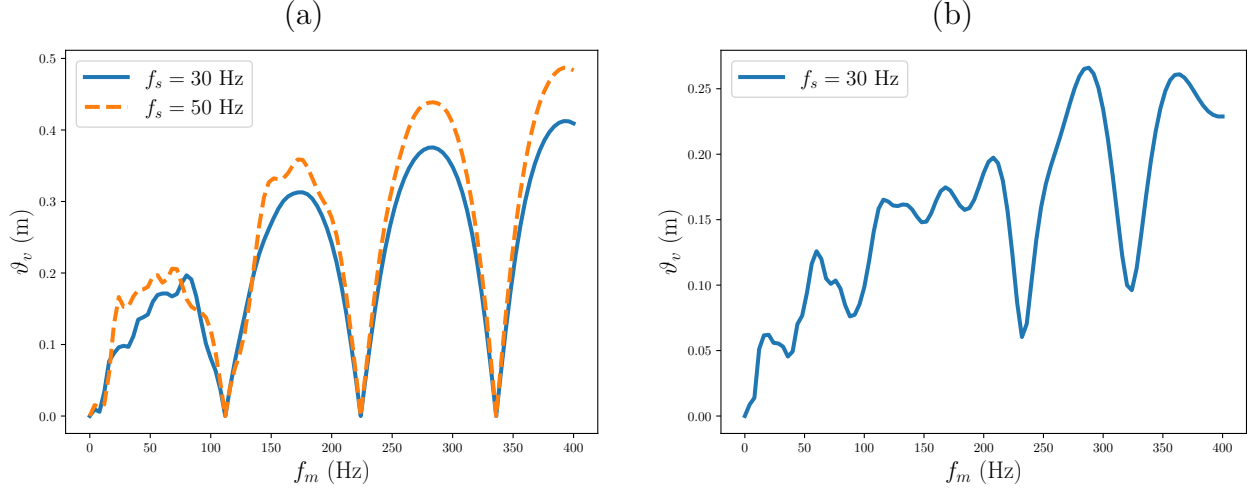


Figure 11: Quantification of non-reciprocity for various modulation frequencies in (37). (a) periodic modulation with two different values of f_c : blue line for 30 Hz and orange dashed line for 50 Hz. (b) quasi-periodic modulation with $f_c = 30$ Hz.

Measurement with a periodic modulation, as the sinusoidal one treated on Figure 11-(a), shows that some frequencies exist, for a couple source/sensor positions, for which $\vartheta_v = 0$. The link between these values is $\ell_s - \ell_r = p \frac{c}{f_m}$, with $p \in \mathbb{Z}$. For these frequencies, the interface is in the same state (because phase-shifted by a temporal period) when the incident wave crosses the interface. In particular, the case $p = 0$ corresponds to a symmetric case and the measures of non-reciprocity are always zero. It is important to notice that the modulation frequencies with zero non-reciprocity do not depend on the source frequency. One can notice that the non-reciprocity tends to increase with the ratio $\frac{f_m}{f_c}$.

Figure 11-(b) corresponds to a quasi-periodic modulation. Except for the case $\ell_s = \ell_r$, there are no longer values of $f_m \neq 0$ for which $\vartheta_v = 0$, so the signals are always different.

5. Conclusion

In this study, we investigated the interaction of waves with an interface whose jump conditions are modulated in time. Numerical methods for temporal simulations have been developed. Numerical experiments have demonstrated and validated our theoretically predicted properties: amplification of the energy, harmonic generation, impedance matching, and non-reciprocity.

We proved that, under the assumptions of Proposition 2 (only one sinusoidally modulated interface parameter, the other parameter being zero), no parametric amplification resonance can occur. That said, we were not able to conclude on this when these assumptions were relaxed.

While mentioning resonance, it is worth noting here that we have only considered non-resonant jump conditions: we assumed that the interface parameters remain finite for all time.

A relaxation of this assumption could be envisaged in the near future, and would allow us, for example, to study the case of Helmholtz resonators whose physical or geometrical properties vary with time [2, 41].

Another natural follow-up to this work is to consider a set of modulated interfaces, in phase or not, and periodically distributed in space. In the case where the wavelength is large compared with the spacing between interfaces, asymptotic homogenization can be applied, generalizing the work carried out in [6] for the case of non-linear but unmodulated interfaces. This work, currently under finalization, will be the subject of a forthcoming publication.

Conflicts of interest

The authors declare no competing financial interest.

Dedication

The manuscript was written through contributions of all authors. All authors have given approval to the final version of the manuscript.

Acknowledgments

M. D. was funded as a post-doctoral researcher by the Institut Mécanique et Ingénierie (Marseille, France). S. G. was funded by UK Research and Innovation (UKRI) under the UK government's Horizon Europe funding guarantee (grant number 10033143).

Appendix A. Scattering coefficients in the unmodulated case

In the absence of modulation ($\mathcal{E}(t) = \mathcal{E}_0$ and $\mathcal{M}(t) = \mathcal{M}_0$), the scattering coefficients can be calculated analytically. The physical parameters are assumed to be piecewise constant:

$$(\rho, c) = \begin{cases} (\rho_0, c_0) & \text{in } \Omega_0 \quad (x < x_0), \\ (\rho_1, c_1) & \text{in } \Omega_1 \quad (x > x_0). \end{cases}$$

Upon introducing the following quantities

$$\begin{aligned} Z_0 &= \rho_0 c_0, & Z_1 &= \rho_1 c_1, & Z_2 &= \rho_0 c_1, \\ Y_0 &= \mathcal{E}_0 Z_0 Z_1 - \mathcal{M}_0, & Y_1 &= \mathcal{E}_0 Z_0 Z_1 + \mathcal{M}_0, & \omega_c^2 &= \frac{\mathcal{E}_0 \mathcal{M}_0}{4}, \end{aligned} \tag{A.1}$$

the reflection coefficient R and the transmission coefficient T at frequency ω are given by

$$\begin{aligned} R(\omega) &= \frac{(Z_1 - Z_0) \left(1 - \left(\frac{\omega}{\omega_c} \right)^2 + \frac{\mathcal{Q}_C \mathcal{Q}_M}{4} \right) - \mathcal{Q}_C Z_0 Z_1 + \mathcal{Q}_M - i\omega \left(Y_0 + \frac{1}{4} (\mathcal{Q}_C \mathcal{M} + \mathcal{Q}_M \mathcal{E}) (Z_1 - Z_0) \right)}{(Z_1 + Z_0) \left(1 - \left(\frac{\omega}{\omega_c} \right)^2 + \frac{\mathcal{Q}_C \mathcal{Q}_M}{4} \right) + \mathcal{Q}_C Z_0 Z_1 + \mathcal{Q}_M + i\omega \left(Y_1 + \frac{1}{4} (\mathcal{Q}_C \mathcal{M} + \mathcal{Q}_M \mathcal{E}) (Z_1 + Z_0) \right)}, \\ T(\omega) &= \frac{2 Z_2 \left(1 + \left(\frac{\omega}{\omega_c} \right)^2 - \frac{\mathcal{Q}_C \mathcal{Q}_M}{4} - i\omega \frac{1}{4} (\mathcal{Q}_C \mathcal{M} + \mathcal{Q}_M \mathcal{E}) \right)}{(Z_1 + Z_0) \left(1 - \left(\frac{\omega}{\omega_c} \right)^2 + \frac{\mathcal{Q}_C \mathcal{Q}_M}{4} \right) + \mathcal{Q}_C Z_0 Z_1 + \mathcal{Q}_M + i\omega \left(Y_1 + \frac{1}{4} (\mathcal{Q}_C \mathcal{M} + \mathcal{Q}_M \mathcal{E}) (Z_1 + Z_0) \right)}. \end{aligned} \tag{A.2}$$

In the particular case where the density and the Young's modulus are constant, the impedance $Z = \rho c = \sqrt{\rho E}$ is constant. Additionally, let us assume that the two following conditions are satisfied

$$\mathcal{M}_0 = Z^2 \mathcal{E}_0, \quad \mathcal{Q}_M = Z^2 \mathcal{Q}_C. \quad (\text{A.3})$$

Then $R(\omega) = 0$: no reflected wave is generated at a static imperfect interface, at any frequency. One recovers the impedance matching condition given in Proposition 3. Moreover, these coefficients can also be obtained by calculating R_0 and T_0 using (22) when the interfaces are static.

Appendix B. Analytical solution of scattered fields

Here we determine the exact solution of (25) with initial data (33). As in Appendix A, the physical parameters are assumed to be piecewise constant. We consider the case where only the interface stiffness is modulated, whereas the interface inertia is taken to be zero ($\mathcal{M}(t) = 0$). The reciprocal case $\mathcal{M}(t) \neq 0$ and $\mathcal{E}(t) = 0$ can be treated in a similar manner. In both cases, the calculation relies on the method of characteristics, illustrated on Figure B.12 and follows the lines of [34].

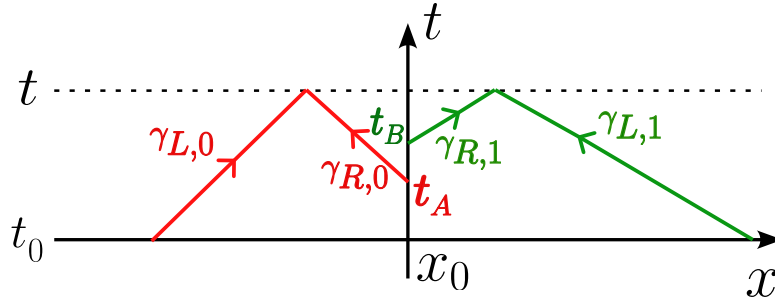


Figure B.12: Principle of the method of characteristics for computing semi-analytical solution using Riemann invariants.

To express $\mathbf{U}(x, t)$ in terms of limit-values of the fields at x_0 , we use the *Riemann invariants* $J^{R,L}$ that are constant along the *characteristics* $\gamma_{R,L}$. The invariants for linear PDEs with constant coefficients satisfy

$$\begin{cases} \gamma_R : \frac{dx}{dt} = +c \Rightarrow \frac{dJ^R}{dt} \Big|_{\gamma_R} = 0, & \text{with } J^R(x, t) = \frac{1}{2} \left(v - \frac{1}{\rho c} \sigma \right) (x, t), \\ \gamma_L : \frac{dx}{dt} = -c \Rightarrow \frac{dJ^L}{dt} \Big|_{\gamma_L} = 0, & \text{with } J^L(x, t) = \frac{1}{2} \left(v + \frac{1}{\rho c} \sigma \right) (x, t). \end{cases} \quad (\text{B.1})$$

Using the continuity of stress (5b) and the invariant (B.1), along with the initial data condition of compact support in Ω_0 , one obtains for $t \geq t_0$

$$\begin{aligned} \sigma^\pm(t) &= -\rho_1 c_1 v^+(t), \\ v^-(t) &= -\frac{\rho_1 c_1}{\rho_0 c_0} v^+(t) + 2 J_0^R(x_0 - c_0 t, 0), \end{aligned} \quad (\text{B.2})$$

where the subscript i on $J_i^{R,L}$ refers to Ω_i . The solution $\mathbf{U}(x, t)$ can be expressed in terms of $v^+(s)$, with $t_0 \leq s \leq t$, and of the initial values of the Riemann invariants. Introducing the

traveltimes

$$t_A = t - \frac{1}{c_0}(x_0 - x), \quad t_B = t - \frac{1}{c_1}(x - x_0),$$

the solution $\mathbf{U}(x, t)$ is given in Ω_0 by

$$\mathbf{U}(x, t) = \begin{pmatrix} 1 & 1 \\ -\rho_0 c_0 & \rho_0 c_0 \end{pmatrix} \begin{pmatrix} J_0^R(x - c_0 t, 0) \\ \Delta_A(x, t) \end{pmatrix}, \quad (\text{B.3})$$

$$\text{with } \Delta_A(x, t) = \begin{cases} -\frac{\rho_1 c_1}{\rho_0 c_0} v^+(t_A) + J_0^R(x_0 - c_0 t_A, 0) & \text{if } t_A \geq 0, \\ J_0^L(x + c_0 t, 0) & \text{otherwise,} \end{cases}$$

and in Ω_1 by

$$\mathbf{U}(x, t) = \begin{pmatrix} 1 \\ -\rho_1 c_1 \end{pmatrix} \Delta_B(x, t), \quad (\text{B.4})$$

$$\text{with } \Delta_B(x, t) = \begin{cases} v^+(t_B) & \text{if } t_B \geq t_0, \\ 0 & \text{otherwise.} \end{cases}$$

To complete the analytical solution, it remains to determine $v^+(t)$. For this purpose, the jump of displacement (5a) is differentiated, leading to

$$v^+(t) - v^-(t) = (\mathcal{C}(t))' \sigma^+(t) + \mathcal{C}(t) \partial_t \sigma^+(t) + \mathcal{Q}_C \sigma^+(t). \quad (\text{B.5})$$

From (B.2), it follows

$$\left(1 + \frac{\rho_1 c_1}{\rho_0 c_0} + \rho_1 c_1 (\mathcal{C}'(t) + \mathcal{Q}_C)\right) v^+(t) - 2 J_0^R(x_0 - c_0 t, 0) = -\rho_1 c_1 \mathcal{C}(t) \partial_t v^+(t). \quad (\text{B.6})$$

Setting

$$y(t) = v^+(t), \quad h(t) = 2 J_0^R(x_0 - c_0 t, 0), \quad (\text{B.7})$$

one obtains the non-autonomous ODE

$$y'(t) = \frac{1}{\rho_1 c_1 \mathcal{C}(t)} \left(h(t) - \left(1 + \frac{\rho_1 c_1}{\rho_0 c_0} + \rho_1 c_1 (\mathcal{C}'(t) + \mathcal{Q}_C)\right) y(t) \right), \quad (\text{B.8})$$

which is integrated by the usual Runge-Kutta 4 method.

The reciprocal case $\mathcal{M}(t) \neq 0$ and $\mathcal{C}(t) = 0$ can be treated using the following expressions:

$$\Delta_A(x, t) = \begin{cases} -\frac{1}{\rho_1 c_1} \sigma^+(t_A) - J_0^R(x_0 - c_0 t_A, 0) & \text{if } t_A \geq t_0, \\ J_0^L(x + c_0 t, 0) & \text{otherwise,} \end{cases} \quad (\text{B.9})$$

$$\Delta_B(x, t) = \begin{cases} -\frac{\sigma^+(t_B)}{\rho_1 c_1} & \text{if } t_B \geq t_0, \\ 0 & \text{otherwise.} \end{cases} \quad (\text{B.10})$$

and by solving

$$z'(t) = -\frac{\rho_1 c_1}{\mathcal{M}(t)} \left(g(t) + \left(1 + \frac{\rho_0 c_0}{\rho_1 c_1} + \frac{(\mathcal{M}'(t) + \mathcal{Q}_M)}{\rho_1 c_1}\right) z(t) \right), \quad (\text{B.11})$$

where

$$z(t) = \sigma^+(t), \quad g(t) = 2 \rho_0 c_0 J_0^R(x_0 - c_0 t, 0). \quad (\text{B.12})$$

Appendix C. Bounded amplification

Here we prove Proposition 2. The assumptions are:

- homogeneous medium, with $\rho_0 c_0 = \rho_1 c_1 = Z$;
- source point at $x_s < x_0$, with a bounded source function S ;
- T -periodic modulation of the compliance (36), with $\phi_C(t + T) = \phi_C(t) = \varphi_c(\Omega t)$ and $T = 2\pi/\Omega$;
- continuity of stress ($\mathcal{M}_0 = 0$ and $\mathcal{Q}_M = 0$). Similar conclusions hold with a modulated inertia and continuity of velocity ($\mathcal{E}_0 = 0$ and $\mathcal{Q}_C = 0$).

The mean of a function $g(t)$ over T is denoted by

$$\bar{g} = \frac{1}{T} \int_0^T g(t) dt. \quad (\text{C.1})$$

We introduce the following Lemma.

Lemma 1. *Consider the Ordinary Differential Equation*

$$y'(t) = \alpha(t) y + \beta(t), \quad (\text{C.2})$$

where $\alpha(t)$ is a T -periodic function, and $\beta(t)$ is bounded. If $\bar{\alpha} \leq 0$, then $y(t)$ is bounded.

Proof. The integrating factor method yields

$$y(t) = e^{A(t)} \left(y_0 + \int_0^t e^{-A(s)} b(s) ds \right), \quad \text{with } A(t) = \int_0^t \alpha(s) ds. \quad (\text{C.3})$$

If $\bar{\alpha} \leq 0$, then $e^{A(t)}$ does not grow exponentially and $y(t)$ is bounded. \square

Following the same lines as in Appendix Appendix B, it can be proven that $y(t) = v^+(t)$ satisfies the ODE

$$y' = a(t) y + b(t), \quad (\text{C.4})$$

with

$$a(t) = -\frac{1}{Z} \frac{2 + Z (\mathcal{E}'(t) + \mathcal{Q}_c)}{\mathcal{E}(t)}, \quad b(t) = -\frac{1}{Z} \frac{S(t)}{\mathcal{E}(t)}. \quad (\text{C.5})$$

The function $a(t)$ is T -periodic, and $b(t)$ is bounded. If $\bar{a} \leq 0$, then the conclusion of Lemma 1 holds and $y(t)$ is bounded. A sufficient condition to get $\bar{a} \leq 0$ is

$$\varphi'_C(t) \geq -\frac{1}{\mathcal{E}_0 \varepsilon_C \Omega} \left(\frac{2}{Z} + \mathcal{Q}_C \right). \quad (\text{C.6})$$

In the case of a sinusoidal modulation $\varphi_C(t) = \sin(t)$, the condition (C.6) is satisfied if

$$\varepsilon_C \Omega \leq \frac{1}{\mathcal{E}_0} \left(\frac{2}{Z} + \mathcal{Q}_C \right), \quad (\text{C.7})$$

which implies $\varepsilon_C = 0$ (static case) or Ω below a critical frequency. In fact (C.6) is sufficient but not necessary. Indeed, let us consider again the modulation $\varphi_C(t) = \sin(t)$. From (C.5), one obtains

$$a(t) = -\frac{1}{Z \mathcal{E}_0} f(t), \quad (\text{C.8})$$

with

$$f(t) = \frac{2 + \mathcal{Q}_C + \gamma \cos(\Omega t)}{1 + \varepsilon_C \sin(\Omega t)}, \quad \gamma = Z \mathcal{E}_0 \varepsilon_C \Omega. \quad (\text{C.9})$$

The mean value of f writes

$$\begin{aligned} \bar{f} &= \frac{1}{T} \int_0^T \frac{2 + \mathcal{Q}_C + \gamma \cos(\Omega t)}{1 + \varepsilon_C \sin(\Omega t)} dt, \\ &= \frac{1}{2\pi} \left((2 + \mathcal{Q}_C) \int_0^{2\pi} \frac{ds}{1 + \varepsilon_C \sin(s)} + \gamma \int_0^{2\pi} \frac{\cos(s)}{1 + \varepsilon_C \sin(s)} ds \right). \end{aligned} \quad (\text{C.10})$$

Classical change of variables, and integration of a periodic function over one period, gives

$$\int_0^{2\pi} \frac{ds}{1 + \varepsilon_C \sin(s)} = \frac{2\pi}{\sqrt{1 - \varepsilon^2}}, \quad \int_0^{2\pi} \frac{\cos(s)}{1 + \varepsilon_C \sin(s)} ds = 0. \quad (\text{C.11})$$

It follows

$$\bar{a} = -\frac{1}{Z \mathcal{E}_0} \frac{2 + \mathcal{Q}_C}{\sqrt{1 - \varepsilon^2}} < 0. \quad (\text{C.12})$$

Lemma 1 implies that the solution of (C.4) is bounded, which concludes the proof.

References

- [1] Ammari, H., Cao, J., and Hiltunen, E. O. (2022). Nonreciprocal wave propagation in space-time modulated media. *Multiscale Modeling & Simulation*, 20(4):1228–1250.
- [2] Ammari, H., Cao, J., Hiltunen, E. O., and Rueff, L. (2023). Transmission properties of time-dependent one-dimensional metamaterials. *Journal of Mathematical Physics*, 64(12):121502.
- [3] Ashkin, A. (1958). Parametric amplification of space charge waves. *Journal of Applied Physics*, 29(12):1646–1651.
- [4] Assier, R. C., Touboul, M., Lombard, B., and Bellis, C. (2020). High-frequency homogenization in periodic media with imperfect interfaces. *Proceedings of the Royal Society A: Mathematical, Physical and Engineering Sciences*, 476(2244):20200402.
- [5] Assier, R. C. and Wu, X. (2014). Linear and weakly nonlinear instability of a premixed curved flame under the influence of its spontaneous acoustic field. *Journal of Fluid Mechanics*, 758:180–220.
- [6] Bellis, C., Lombard, B., Touboul, M., and Assier, R. (2021). Effective dynamics for low-amplitude transient elastic waves in a 1D periodic array of non-linear interfaces. *Journal of the Mechanics and Physics of Solids*, 149:104321.

- [7] Ben Jazia, A., Lombard, B., and Bellis, C. (2014). Wave propagation in a fractional viscoelastic Andrade medium: Diffusive approximation and numerical modeling. *Wave Motion*, 51(6):994–1010.
- [8] Caloz, C. and Deck-Léger, Z.-L. (2019). Spacetime metamaterials—part i: general concepts. *IEEE Transactions on Antennas and Propagation*, 68(3):1569–1582.
- [9] Caloz, C. and Deck-Léger, Z.-L. (2019). Spacetime metamaterials—part ii: Theory and applications. *IEEE Transactions on Antennas and Propagation*, 68(3):1583–1598.
- [10] Cassedy, E. (1967). Dispersion relations in time-space periodic media part II—unstable interactions. *Proceedings of the IEEE*, 55(7):1154–1168.
- [11] Cassedy, E. and Oliner, A. (1963). Dispersion relations in time-space periodic media: Part i—stable interactions. *Proceedings of the IEEE*, 51(10):1342–1359.
- [12] Chu, R. and Tamir, T. (1972). Wave propagation and dispersion in space-time periodic media. In *Proceedings of the Institution of Electrical Engineers*, volume 119, pages 797–806. IET.
- [13] Couder, Y., Protiere, S., Fort, E., and Boudaoud, A. (2005). Walking and orbiting droplets. *Nature*, 437(7056):208–208.
- [14] Craster, R. V. and Guenneau, S. (2024). *Acoustic Metamaterials: Absorption, Cloaking, Imaging, Time-Modulated Media, and Topological Crystals*. Springer Series in Material Science (2nd Edition).
- [15] Croënne, C., Vasseur, J. O., Bou Matar, O., Hladky-Hennion, A.-C., and Dubus, B. (2019). Non-reciprocal behavior of one-dimensional piezoelectric structures with space-time modulated electrical boundary conditions. *Journal of Applied Physics*, 126(14):145108.
- [16] Cullen, A. (1958). A travelling-wave parametric amplifier. *Nature*, 181(4605):332–332.
- [17] Fang, K., Yu, Z., and Fan, S. (2012). Realizing effective magnetic field for photons by controlling the phase of dynamic modulation. *Nature photonics*, 6(11):782–787.
- [18] Fante, R. (1971). Transmission of electromagnetic waves into time-varying media. *IEEE Transactions on Antennas and Propagation*, 19(3):417–424.
- [19] Farhat, M., Guenneau, S., Chen, P.-Y., and Wu, Y. (2021). Spacetime modulation in floating thin elastic plates. *Physical Review B*, 104(1):014308.
- [20] Fink, M. (2016). From loschmidt daemons to time-reversed waves. *Philosophical Transactions of the Royal Society A: Mathematical, Physical and Engineering Sciences*, 374(2069):20150156.
- [21] Galiffi, E., Harwood, A. C., Vezzoli, S., Tirole, R., Alù, A., and Sapienza, R. (2024). Optical coherent perfect absorption and amplification in a time-varying medium.
- [22] Galiffi, E., Tirole, R., Yin, S., Li, H., Vezzoli, S., Huidobro, P. A., Silveirinha, M. G., Sapienza, R., Alù, A., and Pendry, J. B. (2022). Photonics of time-varying media. *Advanced Photonics*, 4(1):014002.

- [23] Harwood, A. C., Vezzoli, S., Raziman, T. V., Hooper, C., Tirole, R., Wu, F., Maier, S. A., Pendry, J. B., Horsley, S. A. R., and Sapienza, R. (2024). Super-luminal synthetic motion with a space-time optical metasurface.
- [24] Huidobro, P., Silveirinha, M., Galiffi, E., and Pendry, J. (2021). Homogenization theory of space-time metamaterials. *Physical Review Applied*, 16(1):014044.
- [25] Huidobro, P. A., Galiffi, E., Guenneau, S., Craster, R. V., and Pendry, J. B. (2019). Fresnel drag in space-time-modulated metamaterials. *Proceedings of the National Academy of Sciences*, 116(50):24943–24948.
- [26] Jensen, J. S. (2009). Space-time topology optimization for one-dimensional wave propagation. *Computer Methods in Applied Mechanics and Engineering*, 198(5-8):705–715.
- [27] Jensen, J. S. (2010). Optimization of space-time material layout for 1d wave propagation with varying mass and stiffness parameters. *Control and Cybernetics*, 39(3):599–614.
- [28] Kim, B. L., Chong, C., Hajarolasvadi, S., Wang, Y., and Daraio, C. (2023). Dynamics of time-modulated, nonlinear phononic lattices. *Physical Review E*, 107(3):034211.
- [29] Kiorpelidis, I., Diakonov, F. K., Theocharis, G., and Pagneux, V. (2024). Transient amplification in stable Floquet media. *Physical Review B*, 110(13):134315.
- [30] Li, Z., Ma, X., Bahrami, A., Deck-Léger, Z.-L., and Caloz, C. (2023). Space-time fresnel prism. *Physical Review Applied*, 20(5):054029.
- [31] Lira, H., Yu, Z., Fan, S., and Lipson, M. (2012). Electrically driven nonreciprocity induced by interband photonic transition on a silicon chip. *Physical review letters*, 109(3):033901.
- [32] Lombard, B. and Piraux, J. (2003). How to Incorporate the Spring-Mass Conditions in Finite-Difference Schemes. *SIAM Journal on Scientific Computing*, 24(4):1379–1407.
- [33] Lombard, B. and Piraux, J. (2006). Numerical modeling of elastic waves across imperfect contacts. *SIAM Journal on Scientific Computing*, 28(1):172–205.
- [34] Lombard, B. and Piraux, J. (2007). Modeling 1-D elastic P-waves in a fractured rock with hyperbolic jump conditions. *Journal of Computational and Applied Mathematics*, 204(2):292–305.
- [35] Lurie, K. A. (2007). *An introduction to the mathematical theory of dynamic materials*, volume 15. Springer.
- [36] Lustig, E., Segal, O., Saha, S., Bordo, E., Chowdhury, S. N., Sharabi, Y., Fleischer, A., Boltasseva, A., Cohen, O., Shalaev, V. M., and Segev, M. (2023). Time-refraction optics with single cycle modulation. *Nanophotonics*, 12(12):2221–2230.
- [37] Lustig, E., Sharabi, Y., and Segev, M. (2018). Topological aspects of photonic time crystals. *Optica*, 5(11):1390.
- [38] Maestre, F., Münch, A., and Pedregal, P. (2007). A spatio-temporal design problem for a damped wave equation. *SIAM Journal on Applied Mathematics*, 68(1):109–132.

- [39] Maestre, F. and Pedregal, P. (2008). Dynamic materials for an optimal design problem under the two-dimensional wave equation. *Discrete and Continuous Dynamical Systems*, 23(3):973–990.
- [40] Malléjac, M. and Fleury, R. (2023a). Scattering from time-modulated transmission-line loads: theory and experiments in acoustics. *Physical Review Applied*, 19(6):064012.
- [41] Malléjac, M. and Fleury, R. (2023b). Scattering from Time-Modulated Transmission-Line Loads: Theory and Experiments in Acoustics. *Physical Review Applied*, 19(6):064012.
- [42] Milton, G. W. and Mattei, O. (2017). Field patterns: a new mathematical object. *Proceedings of the Royal Society A: Mathematical, Physical and Engineering Sciences*, 473(2198):20160819.
- [43] Morgenthaler, F. R. (1958). Velocity modulation of electromagnetic waves. *IRE Transactions on microwave theory and techniques*, 6(2):167–172.
- [44] Moussa, H., Xu, G., Yin, S., Galiffi, E., Ra’di, Y., and Alù, A. (2023). Observation of temporal reflection and broadband frequency translation at photonic time interfaces. *Nature Physics*, 19(6):863–868.
- [45] Movchan, A. B., Movchan, N. V., Jones, I. S., Milton, G. W., and Nguyen, H.-M. (2022). Frontal waves and transmissions for temporal laminates and imperfect chiral interfaces. *Philosophical Transactions of the Royal Society A: Mathematical, Physical and Engineering Sciences*, 380(2231):20210385.
- [46] Nassar, H., Xu, X., Norris, A., and Huang, G. (2017). Modulated phononic crystals: Non-reciprocal wave propagation and willis materials. *Journal of the Mechanics and Physics of Solids*, 101:10–29.
- [47] Nassar, H., Yousefzadeh, B., Fleury, R., Ruzzene, M., Alù, A., Daraio, C., Norris, A. N., Huang, G., and Haberman, M. R. (2020). Nonreciprocity in acoustic and elastic materials. *Nature Reviews Materials*, 5(9):667–685.
- [48] Pham, K. and Maurel, A. (2022). Diffraction grating with space-time modulation. *Journal of Computational Physics*, 469:111528.
- [49] Pu, X., Marzani, A., and Palermo, A. (2024). A multiple scattering formulation for elastic wave propagation in space–time modulated metamaterials. *Journal of Sound and Vibration*, 573:118199.
- [50] Salehi, M., Rahmatian, P., Memarian, M., and Mehrany, K. (2022). Frequency conversion in time-varying graphene microribbon arrays. *Optics Express*, 30(18):32061.
- [51] Sanguinet, W. (2011). The homogenized equations of motion for an activated elastic lamination in plane strain. *ZAMM-Journal of Applied Mathematics and Mechanics/Zeitschrift für Angewandte Mathematik und Mechanik*, 91(12):944–956.
- [52] Swintek, N., Matsuo, S., Runge, K., Vasseur, J. O., Lucas, P., and Deymier, P. A. (2015). Bulk elastic waves with unidirectional backscattering-immune topological states in a time-dependent superlattice. *Journal of Applied Physics*, 118(6):063103.

- [53] Taravati, S. and Caloz, C. (2016). Mixer-duplexer-antenna leaky-wave system based on periodic space-time modulation. *IEEE transactions on antennas and propagation*, 65(2):442–452.
- [54] Tessier Brothelande, S., Croënne, C., Allein, F., Vasseur, J. O., Amberg, M., Giraud, F., and Dubus, B. (2023). Experimental evidence of nonreciprocal propagation in space-time modulated piezoelectric phononic crystals. *Applied Physics Letters*, 123(20):201701.
- [55] Tien, P. K. (1958). Parametric amplification and frequency mixing in propagating circuits. *Journal of Applied Physics*, 29(9):1347–1357.
- [56] Tirole, R., Galiffi, E., Dranczewski, J., Attavar, T., Tilmann, B., Wang, Y.-T., Huidobro, P. A., Alú, A., Pendry, J. B., Maier, S. A., Vezzoli, S., and Sapienza, R. (2022). Saturable time-varying mirror based on an epsilon-near-zero material. *Physical Review Applied*, 18(5):054067.
- [57] To, H. T. (2009). Homogenization of dynamic laminates. *Journal of mathematical analysis and applications*, 354(2):518–538.
- [58] Torrent, D., Parnell, W. J., and Norris, A. N. (2018). Loss compensation in time-dependent elastic metamaterials. *Physical Review B*, 97(1):014105.
- [59] Touboul, M., Lombard, B., Assier, R. C., Guenneau, S., and Craster, R. V. (2024). High-order homogenization of the time-modulated wave equation: non-reciprocity for a single varying parameter. *Proceedings of the Royal Society A: Mathematical, Physical and Engineering Sciences*, 480(2289).
- [60] Touboul, M., Lombard, B., and Bellis, C. (2020). Time-domain simulation of wave propagation across resonant meta-interfaces. *Journal of Computational Physics*, 414:109474.
- [61] Weekes, S. L. (2001). Numerical computation of wave propagation in dynamic materials. *Applied numerical mathematics*, 37(4):417–440.
- [62] Wen, X., Zhu, X., Fan, A., Tam, W. Y., Zhu, J., Wu, H. W., Lemoult, F., Fink, M., and Li, J. (2022). Unidirectional amplification with acoustic non-Hermitian space-time varying metamaterial. *Communications Physics*, 5(1):1–7.
- [63] Yuan, L., Shi, Y., and Fan, S. (2016). Photonic gauge potential in a system with a synthetic frequency dimension. *Optics letters*, 41(4):741–744.
- [64] Zhu, X., Li, J., Shen, C., Peng, X., Song, A., Li, L., and Cummer, S. A. (2020a). Non-reciprocal acoustic transmission via space-time modulated membranes. *Applied Physics Letters*, 116(3):034101.
- [65] Zhu, X., Li, J., Shen, C., Zhang, G., Cummer, S. A., and Li, L. (2020b). Tunable unidirectional compact acoustic amplifier via space-time modulated membranes. *Physical Review B*, 102(2):024309.